Tilla Farnes Hennum

Pile Loading Test in Permafrost

Back Analysis of Settlements Using an Elasto-Viscoplastic Model

January 2023

NTNU
Norwegian University of
Science and Technology
Faculty of Engineering
Department of Civil and Environmental Engineering

Master's thesis

2023

Tilla Farnes Hennum

Master's thesis

NTNU
Norwegian University of
Science and Technology

NTNU
Norwegian University of
Science and Technology

NTNU
Norwegian University of
Science and Technology

Pile Loading Test in Permafrost

Back Analysis of Settlements Using an Elasto-Viscoplastic Model

Tilla Farnes Hennum

Civil and Environmental Engineering
Submission date: January 2023
Supervisor: Professor Gudmund Reidar Eiksund
Co-supervisor: Seyed Ali Ghoreishian Amiri

Norwegian University of Science and Technology
Department of Civil and Environmental Engineering

Preface

This paper is a master's thesis in geotechnical engineering at the Norwegian University of Science and Technology (NTNU) and the final part of the MSc program in Civil and Environmental Engineering. The work was carried out during the autumn semester of 2022 in cooperation with the University Center in Svalbard (UNIS). The main supervisor of the thesis has been Gudmund Reidar Eiksund, and the co-supervisor has been Seyed Ali Ghoreishian Amiri.

Trondheim, 16.01.2023

Tilla Farnes Hennum

Acknowledgement

I would like to thank the following people and institutions for their help during my master's thesis:

Gudmund Reidar Eiksund - For being my supervisor during the project and assisting me throughout the semester.

Seyed Ali Ghoreishian Amiri - For giving me access and guidance to the model used for the simulations and a lot of help throughout the semester.

University Centre in Svalbard (UNIS) - For giving me the opportunity to visit Longyearbyen and view the pile test site.

Aleksey Shestov (UNIS) - For thoroughly explaining the work at Longyearbyen and being my guide during my stay at UNIS.

The Nunataryuk Project - For financially supporting my field trip to Longyearbyen.

My fellow NTNU students and friends - For giving me motivation, help and relevant discussions.

T.F.H

Abstract

Frozen soils generally have a higher compressive strength than the equivalent unfrozen soils, leading to a higher bearing capacity and a lower deformation rate. Due to this, frozen soils have traditionally been a stable and reliable material for foundations. Global warming will inevitably have a large impact on the temperature in Arctic regions; as it is estimated that the temperature in the Arctic will rise by 4-5 °C from the end of the 20th century to 2050 [AMAP, 2017]. This will lead to warming and degradation of the permafrost, giving geotechnical challenges in areas whereby earlier, one could assume a stable, reliable layer of permafrost. The mechanical properties of frozen soils are generally much more temperature dependent than those of unfrozen soils. Warm permafrost, with a ground temperature close to the melting point, is particularly sensitive to temperature change, and a small temperature rise can have a significant impact on the soil conditions. A larger extent of warm permafrost will lead to a bigger uncertainty in the soil conditions, increasing the need for accurate frozen soil models. As the soil conditions are rapidly changing, previous empirical methods will be less relevant and it is expected that the use of numerical models will increase.

In this thesis, an ongoing pile loading test at Longyearbyen, Svalbard, has been investigated. For the test, three end bearing wooden piles have been installed about 4 meters down in the ground, in a permafrost soil layer of marine clay. The piles have step-wise been loaded with concrete slabs and the corresponding settlements have been measured. The experimental data from the test, consisting of temperature- and settlement data from the pile foot, has been gathered. Thereafter, the pile loading test has been simulated using an elasto-viscoplastic numerical soil model in the finite element method program PLAXIS V21.1. The model parameters are largely based upon the research from the doctoral dissertation Lyu [2021] and the parameter values given in Lyu et al. [2021c]. Some modifications and additional numerical calibration were necessary to increase the parameters' accuracy. The model was run for the time period of May 2020 to October 2022.

The results from the PLAXIS simulations show a good correspondence to the experimental data for the total settlements at the pile footing. However, there is a deviation between the experimental and modelled data in creep behaviour throughout the simulated time period. The experimental data shows an immediate settlement after loading, but also a change in creep rate as the ground temperature increases towards -3 °C. The simulations do not show this change in creep behaviour and are heavily dominated by immediate settlements. Some of the discrepancy in creep behaviour can be explained by the formulation of the parameter N, often referred to as the creep ratio. This parameter governs the strain rate sensitivity of the material. In the model formulation, N is given as a linear function of the cryogenic suction and the ice content. Such a linear dependency on the ice content and suction is not an accurate depiction of reality and should be modified to get a better prediction of the temperature dependency of the creep rate.

The simulated temperature at the pile footing varies from -3.3 to -1.8 °C, while the measured temperature varies between -4.1 and -2.7 °C, resulting in an offset of about 0.5 to 1.0 °C over the compared time period. Due to compatibility issues between the given frozen soil model and the PLAXIS software, the latent heat of phase change for water is not accounted for in the simulations, causing most of the observed deviation. Another source of the

deviation is uncertainties in the initial ground thermal regime and thermal boundary conditions.

To conclude, the frozen soil model investigated in this thesis can be used to get an approximate prediction of the expected ground temperature and settlements, which is useful when designing foundations in permafrost areas. It is important to keep in mind that the numerical simulations are an estimate of the future, and cannot be treated as exact knowledge. To account for uncertainties, safety factors in accordance with national regulations must be implemented in the design of foundations.

Sammendrag

Løsmasser i permafrost vil ha en høyere bæreevne og en lavere setningsrate en tilsvarende ikke-frosne løsmasser. Tradisjonelt har derfor løsmasser i permafrost vært et stabilt og pålitelig materiale for fundamentering. Global oppvarming gir stadig varmere temperaturer, og det er estimert at temperaturen i arktiske områder vil stige med 4-5 °C innen 2050 sammenliknet med temperaturen på slutten av 1900-tallet [AMAP, 2017]. Dette vil utvilsomt gi en oppvarming og tilbaketrekning av permafrosten, som vil føre til geotekniske utfordringer i områder hvor man tidligere har kunnet anta en stabil permafrost i løsmassene. De mekaniske egenskapene til frosne løsmasser er generelt mer temperaturavhengige enn tilsvarende ikke-frosne løsmasser. Varm permafrost, hvor temperaturen i grunnen ligger nærme smeltepunktet, er spesielt sensitiv ovenfor temperaturforandringer og en liten temperaturstigning kan ha betydelig innvirkning på grunnforholdene. Et større omfang av varm permafrost vil derfor føre til større usikkerheter i grunnforholdene, som øker behovet for nøyaktige numeriske modeller for løsmasser i permafrost.

I denne masteroppgaven er et pågående pelebelastningsforsøk i Longyearbyen, Svalbard, undersøkt. I forsøket er tre spissbærende trepeler installert omtrent 4 meter ned i grunnen, i permafrost bestående av marin leire. Pelene har trinnvis blitt belastet med betongplater og de tilhørende setningene er målt. Forsøksdata inkludert temperatur- og setningsdata fra peleføttene har blitt innhentet. Deretter er pelebelastningsforsøket blitt simulert ved hjelp av en elasto-viskoplastisk numerisk modell i modelleringsdataprogrammet PLAXIS V21.1. Modellparameterne er hovedsakelig basert på forskningsarbeidet i doktoravhandlingen Lyu [2021] og parameterverdiene som er gitt i Lyu et al. [2021c]. For å forbedre nøyaktigheten til simuleringen er ytterligere numerisk kalibrering og noen modifikasjoner i parameterverdier foretatt. Simuleringen er gjort for perioden fra mai 2020 til oktober 2022.

Resultatene fra PLAXIS simuleringen er i samsvar med innhentet forsøksdata og det er god nøyaktighet mellom de simulerte og målte setningene ved peleføttene. Likevel er det et avvik i den simulerte og observerte krypoppførselen til løsmassene. Målingene viser en umiddelbar setning etter hver lastpåførsel, men også en temperatur- og tidsavhengig krypsetning. Målingene viser at krypraten endres når temperaturen i grunnen stiger mot -3 °C. Simuleringene er i stor grad dominert av umiddelbare setninger etter lastpåførsel, og viser ikke en slik forandring i kryprate. Noe av avviket i krypoppførsel kan skyldes formuleringen av parameteren N, ofte kalt krypforhold (creep ratio). Denne parameteren styrer materialets følsomhet ovenfor tøyningsraten. I den elasto-viskoplastiske modellen er N gitt som en lineær funksjon av isinnholdet og poresuget. En slik lineær avhengighet er ikke en nøyaktig beskrivelse av virkeligheten, og bør forbedres for å få en mer nøyaktig simulering av krypraten.

Den simulerte temperaturen ved pelespissen varier fra -3.3 til -1.8 °C, mens de ekvivalente temperaturmålingene viser en variasjon mellom -4.1 og -2.7 °C, som gir et avvik på omtrent 0.5 til 1.0 °C i løpet av den simulerte tidsperioden. På grunn av kompatibilitetsproblemer mellom den elasto-viskoplastiske modellen og programvaren til PLAXIS vil ikke den latente varmen i faseovergangen mellom vann og is inkluderes i temperaturberegningene. Dette er hovedårsaken til det observerte avviket. En annen kilde til temperaturavviket er usikkerhet rundt initialbetingelsene til det termiske regimet i grunnen og usikkerhet knyttet til de termiske randbetingelsene til modellen.

Alt i alt kan den undersøkte elasto-viskoplastiske modellen brukes for å få et godt estimat av temperaturutviklingen i grunnen og forventede setninger, som er svært nyttig ved dimensjonering av fundamenter i områder med

permafrost. Det er likevel viktig å huske på at numeriske simuleringer, slik som de representert i denne oppgaven, er et anslag og kan derfor ikke behandles som harde fakta. For å ta hensyn til usikkerhet i beregningene er det nødvendig å implementere sikkerhetsfaktorer i fundamenteringsdesignet i tråd med nasjonale retningslinjer.

Contents

Preface i

Acknowledgement ii

Abstract iii

Sammendrag v

Contents **vii**

List of Tables **ix**

List of Figures **xi**

List of Symbols **xii**

1 Introduction **1**

1.1 Background 1

1.2 Scope and Objectives 3

1.3 Limitations 3

1.4 Approach 3

1.5 Structure of the Report 4

2 Theory of Frozen Soils **5**

2.1 Ground Temperature 5

2.2 Permafrost 6

2.2.1 Warm Permafrost 7

2.2.2 Active Layer 8

2.3 Mechanical properties 9

2.3.1 Strength of Frozen Soils 9

2.3.2 Cryogenic Suction and Premelting Mechanisms 10

2.3.3 Creep 12

2.3.4 Phase Change and Latent Heat 13

3 Theory of Frozen Soil Modelling **14**

3.1 Background . . . 14

3.2 Previous Models . . . 15

3.3 Model Formulation . . . 16

3.3.1 Elastic Response . . . 17

3.3.2 Reference, Dynamic and Yield Surfaces . . . 17

3.3.3 Hardening Rules . . . 19

3.3.4 Flow Rules . . . 20

4 Pile Loading Test at Longyearbyen **22**

4.1 Site Background . . . 22

4.2 Experimental Setup of the Pile Loading Test . . . 24

4.3 Preliminary Test Results from the Pile Loading Test . . . 26

5 Numerical Modelling of the Pile Loading Test **30**

5.1 Previous Analysis . . . 30

5.2 Numerical Calibration of Model Parameters . . . 31

5.3 Final Model Parameters . . . 35

5.4 PLAXIS 2D; Model Setup . . . 36

5.4.1 Boundary conditions . . . 39

6 Analysis and Results **41**

6.1 Simulated Settlements . . . 41

6.2 Simulated Temperature . . . 44

7 Discussion **47**

7.1 Assumptions Regarding the Surface Temperature . . . 47

7.2 Simplifications in the Numerical Model . . . 48

7.3 Ground Temperature Deviation . . . 48

7.4 Temperature-dependent Creep Rate . . . 49

7.5 Knowledge of the Numerical Model . . . 50

7.6 Importance of Numerical Modelling of Frozen Soils . . . 51

8 Conclusion **52**

8.1 Summary and Conclusion . . . 52

8.2 Recommendations for Future Work . . . 53

Bibliography **55**

Appendix A - PLAXIS Model; Settings and Results **I**

List of Tables

5.1 Properties of the samples used for triaxial creep tests done by Lyu [2021]. 31
5.2 Calibrated N 33
5.3 Parameters of the two sand layers 35
5.4 Parameters of the marine clay layer 36
5.5 Loading dates and quantities 38

List of Figures

1.1 Estimated permafrost distribution in the period 2000-2014 and 2041-2060 given RCP4.5 scenario. Observed mean annual ground temperatures (MAGT) are marked with coloured circles and obtained from borehole data. Obtained from Hjort et al. [2018]. 2

2.1 Temperature fluctuations as a function of depth (z) in a homogeneous soil (adapted from Andersland and Ladanyi [2004]). 6
2.2 The temperature profile of a frozen soil. The active layer is indicated at the top of the profile. The average ground temperature, T_m, will gradually increase with depth due to the heat flow from within the earth (adapted from Andersland and Ladanyi [2004]). 8
2.3 Coherence between in-situ stresses, σ_m and shear strength, τ, of a frozen soil from triaxial tests. The three phases are given in roman letters above the figure (adapted from Chamberlain et al. [1972]). . . . 10
2.4 Illustration of the difference between curvature induced premelting and interfacial pre-melting. Adapted from Amiri et al. [2016b]. 11
2.5 Creep-curve variations during a constant-stress creep test. Adapted from Andersland and Anderson [1978]. 12

3.1 Illustration of the reference and dynamic surface in the $p^* - S$ and $p^* - q^*$ spaces. Adapted from Amiri et al. [2016a]. 19

4.1 Overview of the pile test site. Figure (a) shows an overview of Svalbard, while Figure (b) shows an overview of the test site. Background maps are obtained from respectively Institute [2022b] and Institute [2022a]. 23
4.2 Illustrated profile of the pile loading test. 24
4.3 Illustrated overview of the pile loading test site 25
4.4 Pictures of the pile loading test after the last loading (12 concrete slabs). 26
4.5 Measured surface temperature of thermistor E5 along with an optimised sinusoidal function of the temperature. 27
4.6 Measurements from each of the piles. 28

5.1 Settings for simulations of undrained triaxial creep test. The duration and number of steps for phase 2 and the increment of $\Delta\sigma_{yy}$ = q varies for the different tests. 32
5.2 Calibration of the strain rate coefficient for the triaxial tests at -3°C. Dashed lines show simulated results, whilst full lines show the laboratory results. 33
5.3 Calibration of the strain rate coefficient for the triaxial tests at -5°C. Dashed lines show the simulated results, whilst full lines show the laboratory results. 34
5.4 An illustration of the soil polygon. Adapted from [Lyu, 2021]. 37
5.5 Function of the unfrozen water content (WU/W0) with respect to temperature for the sand layers. . . . 38
5.6 Profile of the ground temperature at thermistor E5 on the first day of loading. The red point has been disregarded. 40

6.1 Model simulation of the settlements at the pile foot along with data loggers of the settlement at each pile foot. 42
6.2 Model simulation of the settlements at the pile foot along with data measurements from Pile 1 and Pile 3. 42
6.3 Model simulation of the settlements at the pile foot, showing each loading with the total number of added concrete slabs. 43
6.4 Model simulation of the temperature at the pile foot along with data measurements from thermistors at the pile foot. 44
6.5 Temperature boundary condition at the ground surface along with simulated temperature the pile tip. 45
6.6 Simulated temperature with depth at the end of each creep phase. 46

7.1 The strain rate coefficient, N, as a function of temperature 50

1 Phase settings used in PLAXIS calculation. I
2 Modelled soil polygon and element mesh in PLAXIS. II
3 Modelled soil polygon and element mesh around the pile tip. III
4 Vertical displacement around the pile tip for the soil polygon. IV
5 Temperature distribution through the soil polygon at the end of each creep phase, in ascending order from left to right. V

List of Symbols

Greek Symbols

α	Thermal diffusivity of the soil [m^2/s]
β	Parameter controlling the rate of change in soil stiffness with suction [m^2/N]
γ	Plastic potential parameter [-]
δ_{ij}	Kronecker's delta [-]
$\mathbf{d}\epsilon$	Strain increment [-]
$\mathbf{d}\epsilon^{me}$	Increment of elastic strain due to solid phase stress [-]
$\mathbf{d}\epsilon^{mvp}$	Increment of viscoplastic strain due to solid phase stress [-]
$\mathbf{d}\epsilon^{se}$	Increment of elastic strain due to suction variation [-]
$\mathbf{d}\epsilon^{sp}$	Increment of elastic strain due to suction variation [-]
κ	Elastic compressibility coefficient of the soil [-]
κ_0	Unfrozen soil elastic compressibility coefficient [-]
κ_s	Elastic compressibility coefficient for suction variation [-]
λ	Elasto-viscoplastic compressibility coefficient for a frozen state [-]
λ_0	Elasto-viscoplastic compressibility coefficient for unfrozen state [-]
$\mathbf{d}\lambda_1$	Plastic multiplayer regarding the loading collapse reference surface [-]
$\mathbf{d}\lambda_2$	Plastic multiplayer regarding the grain segregation yield surface [-]
λ_r	Parameter for fitting unfrozen saturation curve [-]
λ_s	Elasto-viscoplastic compressibility coefficient for suction variation [-]
μ	Fluidity of the system corresponding to the reference strain rate [1/(Pa·s)]
μ_0	Unfrozen fluidity corresponding to the reference strain rate [1/(Pa·s)]
ν_f	Frozen soil Poisson's ratio [-]
ρ	Density of the soil [kg/m^3]
ρ_i	Density of ice [kg/m^3]
σ	Total stress [N/m^2]
σ'	Effective stress [N/m^2]
σ^*	Solid phase stress [N/m^2]

σ_r^*	Stress point on the loading collapse reference surface [N/m^2]

Latin Symbols

A_s	Amplitude of the surface temperature [K]
b_1	Coefficient for rate of change in N with suction [1/Pa]
b_2	Coefficient for rate of change in N with ice saturation [-]
c_p	Specific heat capacity of the soil [J/(kg·K)]
E_f	Frozen soil Young's modulus [N/m^2]
$E_{f_{ref}}$	Frozen soil Young's modulus at a reference temperature [N/m^2]
$E_{f_{inc}}$	Rate of change in frozen soil Young's modulus with temperature [N/m^2]
F_d	Yield criterion for the dynamic surface [-]
F_{gs}	Yield criterion due to grain segregation [-]
F_r	Yield criterion for the reference surface [-]
e	Void ratio [-]
G	Soil shear modulus [N/m^2]
G_0	Soil shear modulus in unfrozen state [N/m^2]
H	Heaviside function [-]
$\mathbf{I}$	Unit tensor [-]
K	Bulk modulus of the soil [N/m^2]
k	Heat conductivity of the soil [W/(m·K)]
k_{t1}	Parameter for rate of change in apparent cohesion with suction [-]
k_{t2}	Hardening parameter for apparent cohesion [-]
l	Specific latent heat of fusion for water []
M	Slope of the critical state line [-]
N	Creep ratio [-]
N_0	Parameter for strain rate dependency for unfrozen state [-]
p	Time period, either 24 hours or 1 year [s]
p_{at}	Atmospheric pressure [N/m^2]
p_i	Ice pressure [N/m^2]
p_w	Water pressure [N/m^2]
p^*	Current solid phase mean stress [N/m^2]
p_c^*	Reference stress [N/m^2]
p_r^*	Reference effective mean stress [N/m^2]
p_{td}^*	Apparent dynamic cohesion of the soil [N/m^2]
p_{tr}^*	Apparent reference cohesion of the soil [N/m^2]
p_{yd}^*	Dynamic preconsolidation stress [N/m^2]

p^*_{yr}	Reference preconsolidation stress [N/m^2]
p^*_{y0r}	Reference preconsolidation stress for the unfrozen soil [N/m^2]
Q_1	Plastic potential function [-]
q^*	Current solid phase deviatoric stress [N/m^2]
q^*_r	Reference deviatoric stress [N/m^2]
R	Similarity ratio of the dynamic on the reference surface [-]
r	Constant related to maximum stiffness of the soil [-]
S	Cryogenic suction [N/m^2]
S_seg	Initial segregation threshold [N/m^2]
s_w	Unfrozen water saturation [-]
T	Temperature [K]
T_0	Thawing/freezing temperature [K]
T_m	Average annual surface temperature [K]
T_{ref}	Reference Temperature [K]
T_s	Surface temperature [K]
t	Time [s]
z	Depth [m]

Chapter 1

Introduction

1.1 Background

Due to global warming, temperatures are rising. Arctic regions will be deeply affected by global warming, as the temperatures in the Arctic have been increasing twice as fast as globally for the past 50 years. It is estimated that the temperature in Arctic regions will rise by 4-5°C from the end of the 20th century to 2050. Even with a drastic reduction in emissions, this increase in Arctic temperatures is inevitable due to past emissions and ocean heat storage. The temperature rise will lead to massive degradation of the permafrost [AMAP, 2017]. This degradation can be seen in Figure 1.1, where the estimated permafrost distribution for the time periods 2000 - 2014 and 2041 - 2060 is given. In areas with permafrost, the geotechnical conditions are sensitive to environmental change in a way that cannot be compared to anywhere else in the world, resulting in geotechnical challenges which contribute significantly to the economic considerations regarding construction in such areas [Williams and Wallis, 1995]. The temperature of near-surface permafrost in the Arctic has increased by more than 0.5°C since 2007-2009, and the thickness of the active layer has increased in most areas where permafrost is monitored [AMAP, 2017]. Degrading permafrost will present geotechnical challenges and difficult conditions in places where one earlier assumed a stable permafrost when constructing. Degradation of the permafrost will lead to increased settlement rates alongside a reduced bearing capacity, even in areas that only experience a warming of the permafrost and not any thawing. For existing buildings and infrastructure, global warming will result in an increase in both the extent and intensity of permafrost related damage [Williams and Wallis, 1995]. Soils in permafrost generally have a greater bearing capacity and a lower strain rate than the equivalent unfrozen soils, and as such, they have traditionally provided stable and predictable materials for foundations. Due to degrading permafrost, this notion is now challenged. Decreased predictability requires a good understanding of the ground conditions and how the mechanical properties will vary with temperature in frozen soils.

To face these challenges, we must simulate the behaviour of frozen soil with reasonable accuracy using numerical models. For frozen soils, it is convenient to use thermo-hydraulic-mechanical (THM) simulations in Finite

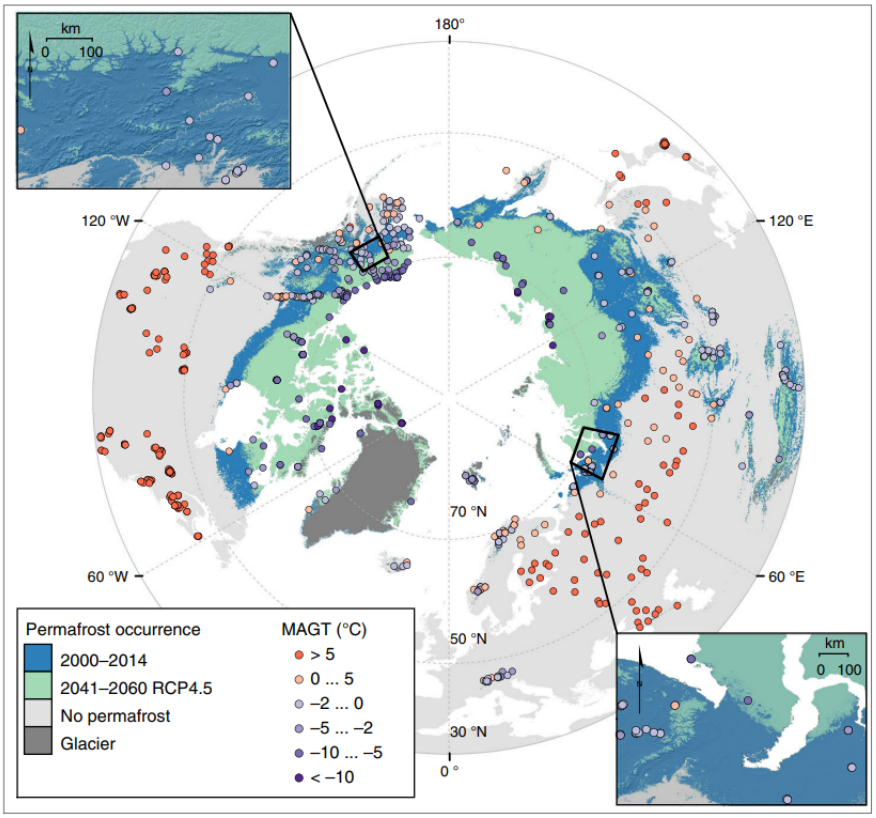

Figure 1.1: Estimated permafrost distribution in the period 2000-2014 and 2041-2060 given RCP4.5 scenario. Observed mean annual ground temperatures (MAGT) are marked with coloured circles and obtained from borehole data. Obtained from Hjort et al. [2018].

Element Models (FEM), due to several complex mechanisms that need to be considered and the non-linearity and mutual coupling of these equations. The majority of conducted geotechnical research concerns unfrozen soils, as it is far more widespread throughout the world. Therefore it is natural that the research and knowledge of unfrozen soils have progressed further. This progression is also aided by the mechanical properties of unfrozen soils with fewer complex mechanisms, such as a lack of temperature dependence, and thus simpler models. For frozen soils however, it is crucial to look at the temperature dependence of the mechanical properties. This leads to several additional complicated mechanisms that need to be considered, making it increasingly challenging to simulate the behaviour correctly.

In recent years several more accurate models for frozen soils have been developed. For example, Nishimura et al. [2009] developed the first two stress-state models for frozen soils. Several others, such as Amiri et al. [2016b], Zhou [2014] have followed. To evaluate the accuracy of the models, it is necessary to compare the simulations with empirical data. In this thesis, an ongoing pile loading test at Longyearbyen, Svalbard, will be simulated using an elasto-viscoplastic frozen soil model developed by Amiri et al. [2016a]. Thereafter the results will be analysed to evaluate if this model can give an acceptable level of accuracy in the pile settlements and temperature variation. This pile loading test has previously been investigated in the PhD dissertation Lyu [2021], where soil samples

from the test area were collected, and thereafter laboratory tests and numerical simulations were carried out. The content of this master's thesis follows the work carried out in the PhD dissertation.

1.2 Scope and Objectives

This master thesis is a numerical study which attempts to simulate the behaviour of frozen soils. The aim is to simulate the deformations and temperature development of an ongoing pile loading test in Longyearbyen, Svalbard, with THM simulations using a finite element model. The research project is a collaboration between UNIS and NTNU. The specific objectives are:

1. To set up a PLAXIS model of the pile loading test, with realistic boundary conditions.
2. To determine model parameters for the numerical model through numerical calibration, using laboratory tests done at samples from the test site.
3. To investigate if the chosen model can simulate the collected data with an acceptable level of accuracy.

1.3 Limitations

Certain simplifications and assumptions have been made during the project. When modelling a boundary value problem of a sediment, the model will be a simplified version of reality. For instance, the different soil layers within the model are assumed to be perfectly homogeneous, which is not physically correct but is necessary to model the soil. In addition, the sand layers are considered to be perfectly linear elastic; therefore, the elasto-viscoplastic soil model has not been used to simulate these layers. The study is limited to a specific test site, whereby samples have been taken from one borehole and logged temperature- and settlement data was collected from three piles placed at the site. The conclusions made from this thesis alone should not be decisive for the application of the model, rather they should be used in context with other papers such as Ghoreishian and Grimstad [2017], which also examines the accuracy of the same frozen soil model. The accuracy of this model is highly dependent on the knowledge and expertise of the user regarding the determination of model parameters and boundary conditions. Therefore, a slight change in input parameters can significantly affect the results, making it hard to get an accurate simulation of the problem if the knowledge about the software is limited. When discussing the consequences of global warming, emphasis is placed on the increase in ground temperature. Other effects of global warming on the ground thermal regime are not considered.

1.4 Approach

The first part of this master thesis is a literary review of the fundamental theory concerning frozen soils and frozen soil modelling. Part of the theory about frozen soils is derived from the project thesis done last semester in the

course TBA4510, which was a literary review of foundations in permafrost and the consequences of global warming [Hennum, 2022]. Based on the data from the pile research project in Longyearbyen, a soil model is constructed and model parameters are decided. From this, THM simulations are done in order to model the behaviour of the frozen soil and finally compare the simulated results with the measured data.

1.5 Structure of the Report

This master thesis consists of 8 chapters structured as follows:

Chapter 1 is an introduction to this master thesis which contains the project's background and the scope and objectives of the thesis. The outline of the report is also presented.

Chapter 2 is a literary review concerning the theory of frozen soils. This is partially an extract from my project thesis in TBA4510 at NTNU, spring 2022 [Hennum, 2022]. The project thesis was a literary review concerning foundations in permafrost and the consequences of global warming.

Chapter 3 gives insight into some of the aspects of numerical models for frozen soils and also provides the model formulation of the chosen numerical model.

Chapter 4 describes the ongoing pile research project in Longyearbyen, Svalbard. It also provides an overview of the gathered data so far.

Chapter 5 outlines the numerical model's setup and the model parameters' determination.

Chapter 6 contains the results and analysis of the frozen soil simulations.

Chapter 7 presents the discussion of the results presented in Chapter 6.

Chapter 8 includes a conclusion of the thesis, a summary of the findings and recommendations for future work.

Chapter 2

Theory of Frozen Soils

This chapter is partially an extract from Hennum [2022], a project thesis written in the course TBA4510, concerning foundations in permafrost and the consequences of global warming. Frozen soils will generally have a higher mechanical strength in compression and therefore have a higher bearing capacity than the corresponding unfrozen soil. The permeability of the frozen soil will be lower than that of unfrozen soil, which prevents seepage. The ice acts as a bonding agent between the particles in the soil, increasing the strength between the particles. The ice will also fill the void between the particles, making it difficult for water to seep through [Andersland and Ladanyi, 2004]. For frozen soils, with a temperature far below the freezing point, a temperature change will not significantly affect the mechanical properties. However, close to the freezing point temperature will considerably impact several of the mechanical properties and be dominant for the design of the foundation [Williams and Wallis, 1995].

2.1 Ground Temperature

The ground's surface temperature depends on the air temperature, the earth's heat conduction, and complicated processes based on the interchange of energy between the atmosphere and the ground. Amongst others, this depends on surface conditions, such as vegetation and topography, and the thermal properties of the soil. When the surface temperature has been decided, the temperature in the ground will be depth- and time-dependent. The variation will depend on the thermal diffusivity of the soil [Williams and Wallis, 1995], and the temperature will vary throughout the day and the year. The average annual temperature on the surface, T_m, and the amplitude of the surface temperature, A_s, can be used to calculate the temperature fluctuations. A common practice is to simulate the surface temperature, T_s, as a sinusoidal function which varies throughout the day or year, as given below.

$$T_{S,t} = T_m + A_s sin\left(\frac{2\pi t}{p}\right) \tag{2.1}$$

where t is the time and p is the simulated period, either 24 hours or a year. The fluctuations in the ground will be attenuated with depth, z, until finally reaching a point where the fluctuations are so small they can be neglected,

and the temperature will be independent of the season. This point is often referred to as ZAA (Zero Annual Amplitude), as given in Figure 2.1. For a homogeneous soil, in a constant phase, the temperature in the ground as a function of time, t, and depth, z, can be estimated as

$$T_{z,t} = T_m + A_s \exp\left(-z\sqrt{\frac{\pi}{\alpha p}}\right) sin\left(\frac{2\pi t}{p} - z\sqrt{\frac{\pi}{\alpha p}}\right) \tag{2.2}$$

where the heat conductivity from the soil is neglected [Andersland and Ladanyi, 2004]. α is the thermal diffusivity of the soil, given as $\alpha = \frac{k}{\rho c_p}$, where k, ρ and c_p are the heat conductivity, density and specific heat capacity of the soil respectively. As a result, there will be a delay between the surface and ground temperatures. Due to this, the warmest temperature further down in the ground will occur in the fall if the warmest surface temperature is during the summer, and the opposite for the coldest temperature. This occurs due to thermal diffusivity, which is an indicator of how fast a temperature change will be transmitted through the soil. It is defined as the ratio of the thermal conductivity to the volumetric heat capacity.

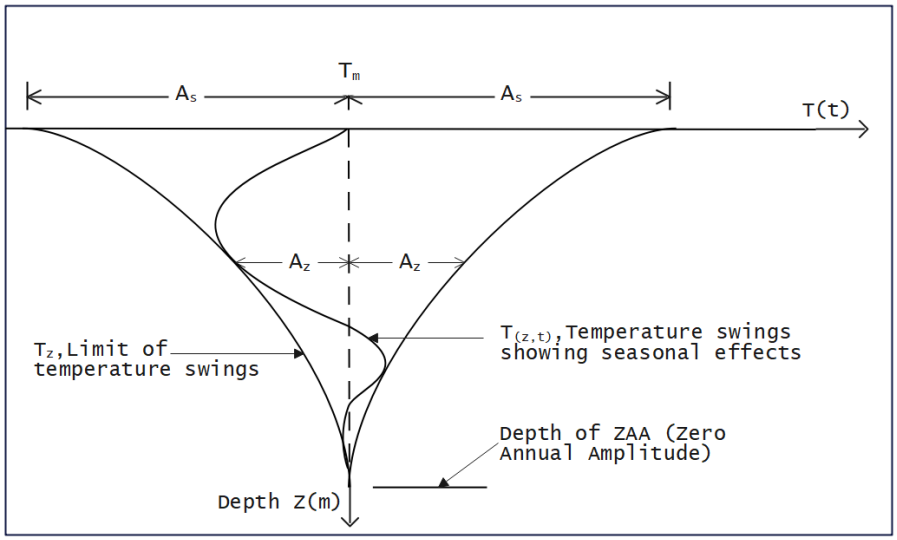

Figure 2.1: Temperature fluctuations as a function of depth (z) in a homogeneous soil (adapted from Andersland and Ladanyi [2004]).

2.2 Permafrost

Permafrost can be defined as soils and rock with a temperature below 0 °C in two consecutive winters and the intermediate summer [Brown and Kupsch, 1974]. As the definition is solely based on temperature and not the physical state of the soil, permafrost is not necessarily completely frozen throughout the year. Salt content, minerals in the soil and pressure can lower the freezing temperature to several degrees below 0 °C. Permafrost can therefore be unfrozen, partially frozen or completely frozen depending on the ice/water saturation according to this definition. In polar regions, permafrost up to 1 km thick can occur. Because of the heat flow from within the earth, there is a limit to how thick the permafrost can become. The average ground temperate will increase with

increasing depth, as shown in Figure 2.2, and at a point becomes higher than the freezing point. Permafrost can be divided into two groups: continuous and discontinuous permafrost. Lakes may affect the thickness of the permafrost on a local lever. It is common to assume that the average surface temperature has to be -3 °C or lower for permafrost to occur [Andersland and Ladanyi, 2004]. The freezing/thawing index can be used as an indicator of permafrost. The freezing (or thawing) index is defined as the total number of degree-days with a surface temperature below (above) 0 °C. A high freezing index combined with a low thawing index will indicate that the area has continuous permafrost. According to Gerdel [1969] a freezing index of minimum 3900 °C days is necessary to obtain continuous permafrost. However, this is only an estimate, as surface vegetation and snow will have an isolating effect influencing the ground temperature and frost depth. On the other hand, if the freezing index is lower than the thawing index, this indicates discontinuous permafrost or no permafrost [Haug Bratlie, 2018, Andersland and Ladanyi, 2004]. Ice-rich permafrost can be defined as permafrost containing excess ice. This means that the ice volume exceeds the soil's total pore volume under natural unfrozen conditions [NSIDC, 2022].

2.2.1 Warm Permafrost

Warm permafrost can be defined as permafrost where the average ground temperature throughout the year is above -1 °C at ZAA [Wang et al., 2020]. Warm permafrost is particularly sensitive to temperature change and disturbance during construction [Wei et al., 2009, Williams and Wallis, 1995]. This is because the ground temperature is close to the freezing temperature, and a slight temperature change may lead to permafrost degradation and an increase in the active layer. Numerical simulations [Riseborough and Smith, 1993] shows that warm permafrost with a thickness of a dozen meter can have significant variations on the location of the freezing zone, one meter or more, during a period of ten years. This is not a consequence of global warming but comes from natural climate variations from year to year and the fact that frozen soils have a higher thermal conductivity than unfrozen soils [Williams and Wallis, 1995]. Because warm permafrost is particularly sensitive to temperature change, both due to global warming, micro-climatic effects and anthropogenic disturbances, the geotechnical design situations can be very demanding. It can be challenging to determine a realistic level for the permafrost, and a slight temperature change can impact the mechanical properties of the soil drastically around the freezing temperature.

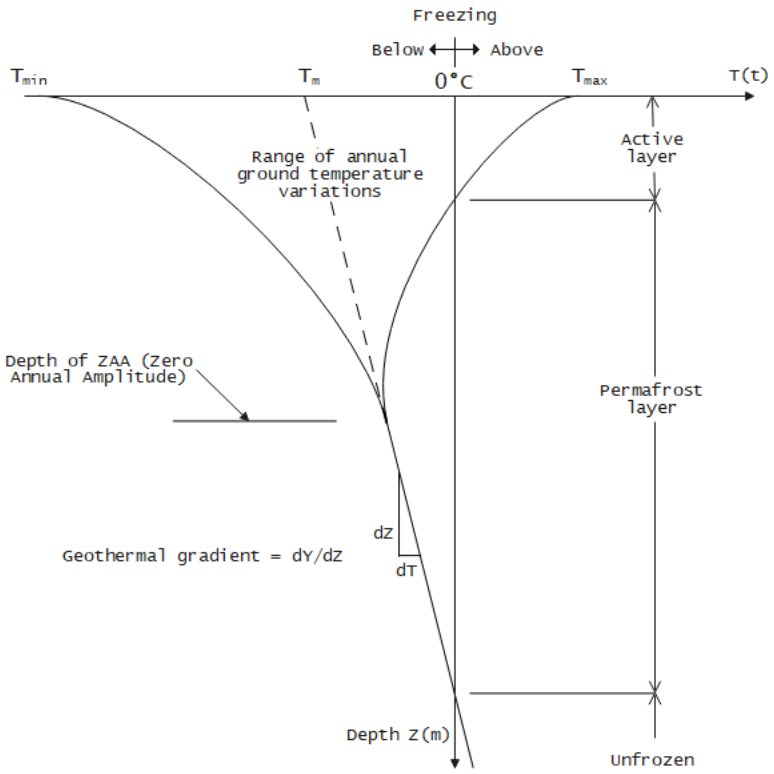

Figure 2.2: The temperature profile of a frozen soil. The active layer is indicated at the top of the profile. The average ground temperature, T_m, will gradually increase with depth due to the heat flow from within the earth (adapted from Andersland and Ladanyi [2004]).

2.2.2 Active Layer

In regions with permafrost, there is an active layer in the soil above the permafrost layer, as shown in Figure 2.2. In the active layer, the temperature will vary above and below the freezing temperature throughout the year. This layer can vary in thickness, from approximately 15 cm in colder regions to several meters in warmer regions. In some areas, there can be a layer of continuous thawed soil between the active layer and the permafrost. This layer is referred to as talik. The freezing front is defined as the line between frozen and unfrozen ground [NSIDC, 2022]. When the soil freezes, the pore water will expand by 9%. This increase in volume will lead to some frost heave [Andersland and Ladanyi, 2004]. However, most of the frost heave is caused by free pore water migrating through capillary action to the freezing front. To achieve equilibrium at the freezing front, the two phases of water, liquid and solid, must be at equilibrium. Solid water (ice) has a lower free energy than liquid water. To maintain equilibrium, free pore water will migrate to the freezing front and consequently freeze to ice. Ice lenses will form and grow throughout the freezing period and create frost heave [French, 2017]. This will occur in frost-susceptible soils, where the capillarity is high, and the permeability is sufficiently large. Silt is known to be especially hazardous for frost heave. During frost heave, the surface will elevate. Since the soil will never be completely homogeneous, ice lenses will lead to surface irregularities which can create problems and damage to infrastructure and foundations.

When the active layer thaws, known as spring thaw, the ice will disappear, leaving excess water in the soil. For fine-grained materials this will, in many situations, exceed the amount of water the soil can absorb and drain, giving an extraordinarily high pore pressure. During rapid thawing, the water cannot be drained, as it is blocked by ice in underlying frozen layers. The soil will be transformed into a muddy mixture of soil particles and water with a low bearing capacity. This may damage infrastructure and foundations overlying the active layer [Andersland and Ladanyi, 2004].

2.3 Mechanical properties

Frozen soils exist of four main components: solid grains, ice, free pore water and gasses [Andersland and Ladanyi, 2004]. The mechanical properties include strength properties based upon cohesion and friction angle amongst others, and stiffness properties dependent on, amongst others, Young's modulus and Poisson's ratio. The main difference from unfrozen soils is that the mechanical properties will be more temperature-dependent in frozen soils. Additionally, the mechanical properties depend on the soil type, the in-situ stresses, ice content, salt content, strain rate and the amount of free pore water. In this thesis, emphasis is primarily placed on how the mechanical properties vary with temperature.

The transition between the solid and liquid phase of water is the leading cause of the specific properties and behaviours of soils in permafrost regions. The transition between the two phases will occur not only at the freezing temperature but also at lower temperatures. This is because there is no clear distinction between the two phases [Williams and Wallis, 1995].

2.3.1 Strength of Frozen Soils

The strength of the soil is determined by the shear strength, which is a mechanical property. Similarly as in unfrozen soils, the shear strength will be compiled by the friction force between the soil particles, the bond between the particles, the cohesion and dilatancy effects. Additionally, the shear strength will have a contribution from the frozen state.

The shear strength will depend on the temperature, in-situ stresses, salt content and strain rate. The strength will increase with decreasing temperatures, as falling temperatures will give harder soils and a higher ice content, contributing to increased strength. In Lyu [2021] experiments indicating that the strength of fine-grained frozen soils varies approximately linear with respect to temperature are shown. For coarse-grained soils however, the experiments indicate that the strength will gradually increase until -6 °C. From this point, the strength increases faster with decreasing temperature. An increase in salt content will give more free pore water as the freezing temperature of the ice will decrease and result in lower shear strength. The shear strength of frozen soils will to a greater extent depend on the strain rate than for unfrozen soils. The reason for this is that the strength of the ice is more sensitive with respect to strain rate than the soil strength. Simultaneously, decreasing temperatures will make the ice strength less dependent on the strain rate [Lyu, 2021]. In conclusion, frozen soils' strength will depend more on

the strain rate than unfrozen soil, but the dependency will decrease with decreasing temperatures. The coherence between in-situ stresses and the shear strength can be described as an effect of three phases, as shown in Figure 2.3. In the first phase (phase I), the shear strength will increase with increasing in-situ stresses, similar to in unfrozen soils. In frozen soil, one will reach a point where the in-situ stresses become big enough for the ice to crush and melt, decreasing the shear strength. This is known as pressure melting and phase II. In phase III, increasing in-situ stresses will increase effective stresses, raising the shear strength of the soil [Chamberlain et al., 1972].

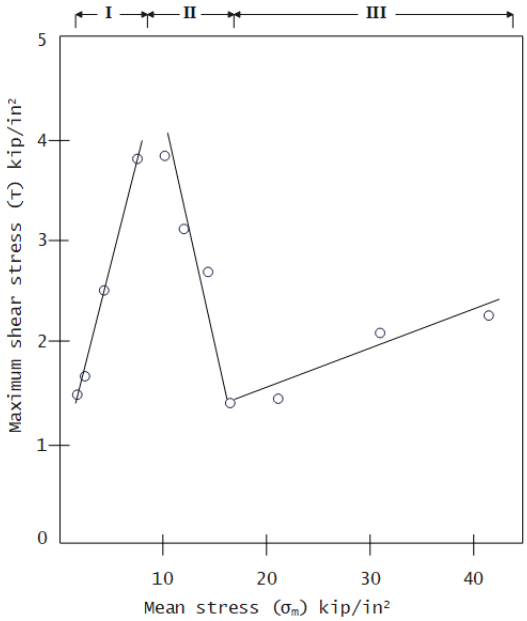

Figure 2.3: Coherence between in-situ stresses, σ_m and shear strength, τ, of a frozen soil from triaxial tests. The three phases are given in roman letters above the figure (adapted from Chamberlain et al. [1972]).

2.3.2 Cryogenic Suction and Premelting Mechanisms

Cryogenic suction is when water migrates to the freezing zone to maintain equilibrium. When water freezes to ice, a negative pressure will occur in the soil. This is because ice has a lower free energy than liquid water, as explained in Section 2.2.2. To maintain energy equilibrium, free water will therefore migrate to the freezing area, causing cryogenic suction [Andersland and Ladanyi, 2004]. The cryogenic suction can be calculated as Equation 2.3, by using the Clausius-Clapeyron equation as a requirement for equilibrium between solid ice and liquid water [Thomas et al., 2009].

$$S = p_i - p_w = -\rho_i l \ln \frac{T}{T_0} \tag{2.3}$$

where S is the cryogenic suction, p_i and p_w is the pressure of ice and water respectfully, while ρ_i denotes the density of ice and l is the specific latent heat of fusion. T is the given temperature, while T_0 is the thawing/freezing temperature of ice/water at the given pressure. Both temperatures are given in kelvin. Equation 2.3 shows that a temperature variation will give a variation in cryogenic suction, and that the cryogenic suction increases with

a reduction in temperature. Since ice content can be described as a function of temperature, it can indirectly be represented as a function of the cryogenic suction [Amiri et al., 2016b]. Therefore, the effect of cryogenic suction is decisive in understanding the mechanisms of frozen soils. Pressure melting, as described in Section 2.3.1, will decrease cryogenic suction and increase water pressure, as the thawing temperature of the ice will be lowered [Amiri et al., 2016b].

According to Wettlaufer and Worster [2006], two mechanisms mainly control the behaviour of ice content and temperature variations: curvature-induced premelting and interfacial premelting. In addition to the salt content, these two mechanisms are the reason why unfrozen water content can exist under the freezing temperature in frozen soils. Curvature-induced premelting results from surface tension and acts similar to suction, bonding the grains together, while interfacial premelting results from disjoining pressure. This is a repelling force between solid grains and ice which normally widens the gap between the grains by sucking in more water [Amiri et al., 2016b]. The difference is illustrated in Figure 2.4. Interfacial premelting is the main difference between capillarity and cryogenic suction. Together the two premelting mechanisms will control the behaviour regarding temperature and ice content variations.

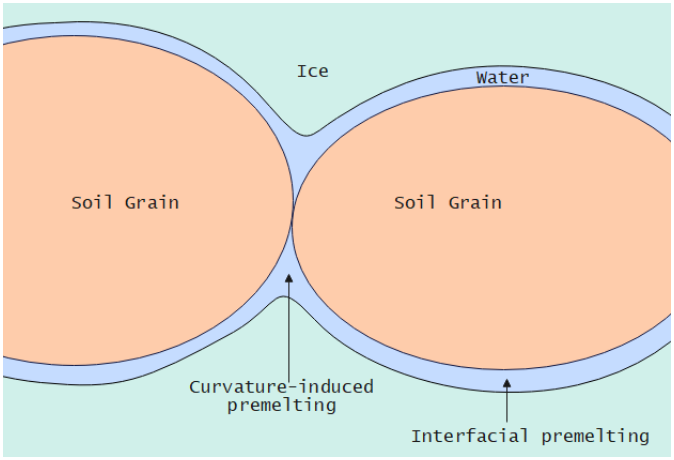

Figure 2.4: Illustration of the difference between curvature induced premelting and interfacial pre-melting. Adapted from Amiri et al. [2016b].

It has been shown through experimental results that the strength of the frozen soil will increase with increasing ice content up to a certain point. After this, the strength will decrease with increasing ice content [Baker, 1979]. This can be described by the premelting mechanisms explained above. The curvature-induced premelting dominates at lower ice content, which gives a positive correlation between the ice content and soil strength. For higher values of ice content however, the interfacial premelting will dominate. Due to grain segregation, the soil strength will therefore decrease. For the interfacial premelting to be dominant, there must be available water, as the mechanism works by sucking in more water between the grains, causing grain segregation [Amiri et al., 2016b].

2.3.3 Creep

Creep deformations are time-dependent deformations that occur over a long period of constant loading. Creep depends on the soil type, density, ice content, temperature and the stress- and strain history of the soil [Huang, 2020]. The deformations can lead to the decomposition and redistribution of the soil particles. Creep deformations can be separated into three categories based on time intervals: primary, secondary and tertiary creep, as shown in Figure 2.5. The rate of creep will respectively decrease, held approximately constant and increase for the three categories. Primary creep will dominate for ice-poor soils, such as fully saturated frozen sand and medium- to high-density silt, under low in-situ stresses. For ice-rich soils, the period of primary creep will be very short and can often be neglected. Instead, secondary creep will dominate, while tertiary creep will not occur [Andersland and Ladanyi, 2004].

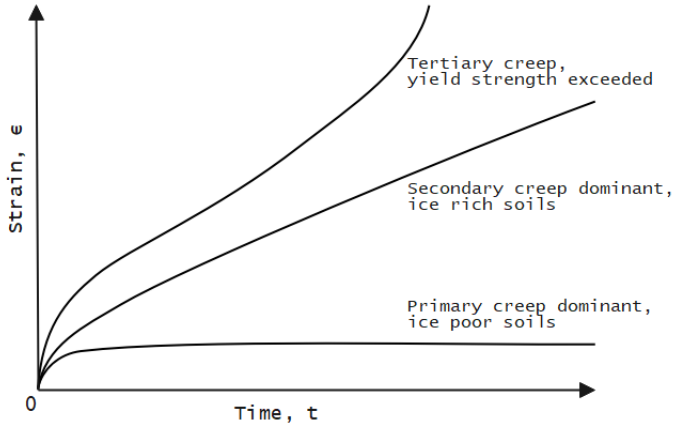

Figure 2.5: Creep-curve variations during a constant-stress creep test. Adapted from Andersland and Anderson [1978].

In frozen soils, the long-term deformations are dominated by creep, and not consolidation. The explanation is that consolidation occurs when free pore water is pushed out of the soil, compressing the soil and causing deformations. When a big part of the pore water is frozen, this phenomenon will not occur to the same extent. However, for soils in warm permafrost where the amount of free pore water may be substantial, the consolidation can have a significant effect that should be considered [Andersland and Ladanyi, 2004]. According to Vyalov and Porkhaev [1976], this applies to silty sand with temperature T > -0.3 °C and clay with T > -1.5 °C.

The creep rate is dependent on temperature. Similarly to how the creep strain rate will increase when applied to a surcharge load, the creep rate will increase with increasing temperature. When the ground temperature varies, one can expect a change in the creep rate. Therefore, the creep rate can have annual variations due to annual temperature fluctuations and a long-time progression due to global warming. The creep behaviour of frozen soils has been a central focus area when it comes to frozen soil research, and a large number of experiments have been done [Yao et al., 2018]. However, most of these focus on how the creep behaviour is affected by variations in the stress state under a constant temperature, and not how the creep behaviour will vary with temperature. During the last decades, a significant increase in ground temperature has been observed, leading to permafrost degradation

[AMAP, 2017]. In areas where the permafrost previously has been cold and stable warmer layers of permafrost are forming, resulting in significant creep settlements. Including the contribution from creep settlements for infrastructure foundations in cold regions where deformations need to be strictly controlled is essential. Therefore it is necessary with precise predictions of the creep settlement when designing permafrost foundations to prevent settlement damages [Yao et al., 2018].

2.3.4 Phase Change and Latent Heat

Ice formation in soils depends on the cooling of a soil-water system. This cooling will not be linear in regards to temperature and time [Andersland and Ladanyi, 2004]. As mentioned in Section 2.2.2 the free energy of ice is lower than that of liquid water. Energy will therefore be released when water goes from liquid to solid phase. This phenomenon is called latent heat. Latent heat is defined as energy released or absorbed by a body during a constant temperature process. The latent heat from the pore water transition is essential when determining the temperature field in frozen soils. The predicted temperature field's accuracy will depend on the accuracy of the phase change estimate [Chen et al., 2021]. The phase change energy is determined by the latent heat of fusion for water, l, given as 333.7 kJ/kg while the specific heat capacity of water is 4.218 kJ/(kg·°C) at 0 °C [Andersland and Ladanyi, 2004]. Consequently, melting 1 kilogram of ice to liquid water at 0 °C requires about 80 times as much energy as heating 1 kilogram of liquid water from 0 to 1 °C. The soil's cryogenic suction will depend on the latent heat of fusion for water, as seen in equation 2.3. During the freezing process, the pore water in the soil is freezing in an extended range of temperatures below 0 °C. In this temperature range, liquid water is continuously transformed into solid ice and releases latent heat [Chen et al., 2021]. For fine-grained soils such as clay, all the free water in the soil pores and the bound water, i.e. unfrozen water film on the soil particles, will not be frozen before approximately -70 °C [Andersland and Ladanyi, 2004]. As pore water freezes it will be separated into freshwater crystals and saltier water. As the process continues the remaining water will become more and more saturated with salt, lowering the freezing temperature. The latent heat will be nonlinear due to the non-linearity of the suction and water saturation. The difficulty and complexity of temperature prediction in frozen soils are increasing due to the phase change of water in the soil freezing process, compared to temperature change in conventional material without phase change [Chen et al., 2021].

Chapter 3

Theory of Frozen Soil Modelling

3.1 Background

The behaviour of frozen soils is governed by several additional complex mechanisms compared to unfrozen soils, all of which need to be considered when simulating the soil behaviour. This makes it more complicated and challenging to create accurate models for frozen soils, especially at the threshold between unfrozen and frozen soils [Nishimura et al., 2009]. Due to global warming, there is an increasing interest in developing accurate models for frozen soils and predicting the expected change in soil strength and deformations as a consequence of temperature rise. As mentioned in Section 2.3 the mechanical properties of frozen soils are highly sensitive to temperature variations as compared to unfrozen soils. Therefore, it is even more necessary to have accurate models which predict the behaviour with an acceptable error. Unlike traditional models for unfrozen soils, a model for frozen soils needs to be able to simulate the influence of ice content and temperature on the mechanical properties of the soil, as the mechanical behaviour will be strongly affected by the amount of ice. This mechanical behaviour is not only dependent on the temperature but also the applied mechanical stresses [Amiri et al., 2016a]. As mentioned in Section 2.3, the behaviour of frozen soils will generally be more rate-sensitive than that of unfrozen soils, as ice is highly rate-dependent. Freezing and thawing of the soil involve complicated thermal, hydraulic and mechanical processes, which can interact with each other and thus influence the geotechnical behaviours of the soil. For instance, phase changes in pore fluids due to temperature variations will modify the hydraulic regime of the soil. This will cause mechanical deformations of the soil. Similarly, any changes in hydraulic or mechanical conditions will affect the thermal processes through advection and changes in ice and water content. Thermo-hydro-mechanical (THM) interactions like these are an essential factor when simulating the behaviour of frozen soils, especially during freezing and thawing periods. Due to these equations' non-linearity and mutual coupling, a finite element method (FEM) must be used to simulate the soil [Nishimura et al., 2009].

In this master thesis, an elastic-viscoplastic model proposed by Amiri et al. [2016a] is used to simulate the frozen soil. The model is formulated as a two stress-state model, using the cryogenic suction and the solid phase stress as

the two independent variables.

3.2 Previous Models

Traditionally total stress models have been widely used to simulate the mechanical behaviour of frozen soils, such as Arenson and Springman [2005], Lai et al. [2008], Zhu et al. [2010]. The main focus of these models is how the confining pressure affects the elastoplastic behaviour. These models focus less on how the other important factors, such as ice content and temperature, influence the behaviour. Because of this, the model can simulate the behaviour due to external loads but cannot simulate settlements when the ice content and/or the temperature varies, such as during a thawing or freezing period. It is also challenging to simulate the behaviour of the soil concerning the unfrozen water content when using total stress-based models [Amiri et al., 2016b].

An alternative is to use a model based on effective stress, defining effective stress as total stress minus pore pressure. Several approaches have been made, by Nixon [1991], Nicolsky et al. [2008], Li et al. [2008], Thomas et al. [2009] amongst others. The pore pressure can be simulated in several ways: as a combination of the ice pressure and unfrozen water pressure or by separating the water and ice pressure. The ice phase is considered as an additional fluid phase and its shear strength is therefore neglected, as fluid phases such as water have approximately zero shear strength [Amiri et al., 2016a]. Effective stress models can simulate the phenomenon of ice segregation during a freezing period with acceptable accuracy, but the soil strength after ice segregation will not be accurate [Amiri et al., 2016b].

A two stress-state method was first proposed by Nishimura et al. [2009] by using the net stress and the cryogenic suction as the two stress variables. The net stress is defined as the excess of total stress over the ice pressure. In this model, the contribution of shear strength from the ice phase is partly taken into account by increasing the yield surface with increasing cryogenic suction, and hence with sinking temperatures [Amiri et al., 2016a]. The model can simulate both thawing and freezing periods. The curvature-induced premelting mechanism, as mentioned in Section 2.3, is also considered in the model. However, the interfacial premelting mechanism is not considered. This mechanism is the central distinction between capillarity and cryogenic suction. Due to this, a problem with the model arises when soils that have already experienced tensile failure, due to decreasing temperature under isotropic stress conditions, are shearing. The soils will then always have dilatant behaviour during shearing. In an unfrozen state, the model will be reduced to an effective stress-based critical state model, by replacing ice pressure with water pressure in the definition of net stress [Amiri et al., 2016b].

Other two-stress models have been suggested later on. For example, Zhou [2014] suggested replacing suction with temperature as the second variable in the model. However, the problem concerning shearing after freezing during isotropic conditions remains [Amiri et al., 2016b]. Zhang and Michalowski [2015] introduced a model using the effective stress and the pore ice ratio as the two independent variables. The pore ice ratio is defined as the ratio of ice volume to the volume of solid particles. A problem with this model is that the definition used for the effective stress will cause an unrealistically high effective confining pressure when the unfrozen water content approaches

zero [Amiri et al., 2016a].

Amiri et al. [2016b] proposed an elastic-plastic two stress-state model, using the solid phase stress and the cryogenic suction as the two variables. The solid phase stress is defined as the total stress in the soil grains and ice. Therefore, the solid phase stress indirectly considers the contribution from the shear strength of the ice phase. In addition, the curvature induced premelting mechanism is also taken into account through the solid phase stress, similar to the Nishimura et al. [2009] model.

3.3 Model Formulation

The model used in this master thesis is based on the elastic-plastic model proposed by Amiri et al. [2016b] and developed further into an elastic-viscoplastic model, as given in Amiri et al. [2016a]. The following section is based on the article by Amiri et al. [2016a], and all formulas are obtained from there. In the same way as the elastic-plastic model in Amiri et al. [2016b], the following model is a two stress-state model, using the solid phase stress and the cryogenic suction as the two variables. The formula and the following description of the cryogenic suction were introduced in Section 2.3.2 by Equation 2.3, which is repeated below

$$S = p_i - p_w = -\rho_i l \ln \frac{T}{T_0} \tag{2.3}$$

Ice crystals are, in this model, considered as a part of the solid phase, which makes it possible to view the fully saturated frozen soil as a porous material where the pores are filled with water. To implement this in the model, a kind of effective stress named the "solid phase stress" is defined [Amiri et al., 2016b], and is given as

$$\boldsymbol{\sigma}^* = \boldsymbol{\sigma} - s_w \rho_w \boldsymbol{I} \tag{3.1}$$

where $\boldsymbol{\sigma}^*$ is the solid phase stress, $\boldsymbol{\sigma}$ is the total stress, s_w is the unfrozen water saturation (ratio of the unfrozen water volume to the total volume of frozen and unfrozen water), $\mathbf{I}$ is the unit tensor and S is the cryogenic suction. By this definition, the solid phase stress is the combined stress from soil grains and ice. This definition differs from the traditionally used Terzhagi's definition of effective stress: $\boldsymbol{\sigma}' = \boldsymbol{\sigma} - \rho_w \boldsymbol{I}$, by including the water saturation, s_w. This is done to account for the frozen ice content, s_i, given as $s_i = 1 - s_w$ assuming the soil is fully saturated.

In the model, strain increments are decomposed into a contribution from the variation in solid phase stress and cryogenic suction. It is assumed that the strain contribution from the solid phase stress variation will exhibit an elastic-viscoplastic behaviour. In contrast, the strain contribution from the cryogenic suction variation will have an elastic-plastic behaviour. Based on this, any strain increment, $d\epsilon$, can be decomposed and expressed as

$$\mathrm{d}\varepsilon = \mathrm{d}\varepsilon^{me} + \mathrm{d}\varepsilon^{mvp} + \mathrm{d}\varepsilon^{se} + \mathrm{d}\varepsilon^{sp} \tag{3.2}$$

where $d\varepsilon^{me}$ and $d\varepsilon^{mvp}$ denote the elastic and viscoplastic contributions from the solid phase stress variation, whilst $d\varepsilon^{se}$ and $d\varepsilon^{sp}$ denote the elastic and plastic contributions from the cryogenic suction variation.

3.3.1 Elastic Response

The elastic part of the strain due to the solid phase stress variation, ε^{me}, can be calculated based on the equivalent shear modulus, G, and the bulk modulus, K:

$$\varepsilon_{ij} = \frac{1}{2G}\sigma_{ij} - \frac{3K-2G}{18KG}\sigma_{kk}\delta_{ij} \tag{3.3}$$

where δ_{ij} is the Kronecker's delta. G and K are given respectively as

$$G = (1-s_i)G_0 + \frac{s_i E_f}{2(1+\upsilon_f)} \tag{3.4}$$

$$K = (1-s_i)\frac{(1+e)p^*}{\kappa_0} + \frac{s_i E_f}{3(1-2\upsilon_f)} \tag{3.5}$$

where G_0 and κ_0 denote the unfrozen soil's shear modulus and the elastic compressibility coefficient respectively, whilst e is the void ratio. p^* is the solid phase mean stress, E_f and υ_f are, respectively, the Young's modulus and the Poisson's ratio of the fully frozen soil, and finally s_i is the ice saturation. The Young's modulus, E_f, will be temperature-dependent and can be expressed as:

$$E_f = E_{f_{ref}} - E_{f_{inc}}(T - T_{ref}) \tag{3.6}$$

where T_{ref} is the reference temperature and $E_{f_{ref}}$ is the corresponding value of E_f at this point. $E_{f_{inc}}$ denotes the rate of change in E_f with temperature. The elastic strain due to the cryogenic suction variation can be expressed as:

$$\mathrm{d}\varepsilon^{se} = \frac{\kappa_s}{3(1+e)} \times \frac{dS}{(S+p_{at})}\mathbf{I} \tag{3.7}$$

where κ_s is the compressibility coefficient due to the suction variation in the elastic region and p_{at} is the atmospheric pressure.

3.3.2 Reference, Dynamic and Yield Surfaces

When the cryogenic suction approaches zero, the model will be reduced to the Modified Cam Clay model for unfrozen soils. For the frozen state, the model is defined by two surfaces: the loading collapse reference surface and the loading collapse dynamic surface, and not a common yield surface. This method is referred to as the overstress method [Perzyna, 1966] and is used to describe soils with an elastic-viscoplastic behaviour. The inelastic deformation can then be calculated by the distance to these two surfaces. The formula for the reference surface has been adopted from previous research [Nishimura et al., 2009, Alonso et al., 1990] and is given as

$$F_r = \left[p_r^* - \left(\frac{p_{yr}^* + p_{tr}^*}{2}\right)\right]^2 + \left(\frac{q_r^*}{M}\right)^2 - \left(\frac{p_{yr}^* - p_{tr}^*}{2}\right)^2 = 0 \tag{3.8}$$

where

$$p_r^* = \frac{(\sigma_r^*)_{11} + (\sigma_r^*)_{22} + (\sigma_r^*)_{33}}{3} \tag{3.9}$$

$$q_r^* = \sqrt{\frac{1}{2}\left[\left((\sigma_r^*)_{11} - (\sigma_r^*)_{22}\right)^2 + \left((\sigma_r^*)_{11} - (\sigma_r^*)_{33}\right)^2 + \left((\sigma_r^*)_{33} - (\sigma_r^*)_{22}\right)^2 - 6\left((\tau_r)_{12}^2 + (\tau_r)_{13}^2 + (\tau_r)_{23}^2\right)\right]} \tag{3.10}$$

$$p_{yr}^* = p_c^* \left(\frac{p_{y_{0r}}^*}{p_c^*}\right)^{\frac{\lambda_0 - \kappa}{\lambda - \kappa}} \tag{3.11}$$

$$\lambda = \lambda_0 \left[(1-r)\exp(-\beta S) + r\right] \tag{3.12}$$

$$\kappa = \frac{1+e}{K} p^*. \tag{3.13}$$

Here σ_r^* indicates a stress point on the loading collapse reference surface, M is the slope of the critical state line, p_{tr}^* denotes the apparent cohesion of the soil, p_c^* is the reference stress, $p_{y_{0r}}^*$ is the reference preconsolidation stress of the unfrozen soil, κ and λ_0 indicate the compressibility coefficient within the elastic region and the compressibility coefficient for the unfrozen state along the virgin loading, respectively. r represents a constant related to the maximum stiffness of the soil, given infinite cryogenic suction, while β is a parameter dependent on the rate of change in the soil stiffness with suction. The loading collapse dynamic surface has a similar line to the reference surface given by $S = 0$. In addition, the dynamic surface should always go through the current stress state (provided by p^*, q^* and S). The dynamic surface is therefore given as

$$F_d = \left[p^* - \left(\frac{p_{yd}^* + p_{td}^*}{2}\right)\right]^2 + \left(\frac{q^*}{M}\right)^2 - \left(\frac{p_{yd}^* - p_{td}^*}{2}\right)^2 = 0 \tag{3.14}$$

where

$$p_{yd}^* = R \cdot p_{yr}^* \tag{3.15}$$

$$p_{td}^* = R \cdot p_{tr}^*. \tag{3.16}$$

In the above equations, q^* and p^* are the solid phase deviatoric and the mean stress, respectively, whilst R is the similarity ratio of the dynamic on the reference surface, given as $R = \frac{p_{yd}^*}{p_{yr}^*}$. To describe the grain segregation phenomenon mentioned in Section 2.3, an elastic-plastic yield criterion is implemented as

$$F_{gs} = S - S_{seg} = 0 \tag{3.17}$$

where S_{seg} is the threshold value of suction for the ice segregation phenomenon. An illustration of the reference and dynamic surfaces is given in Figure 3.1. The dynamic surface will vary with the solid phase stress, increasing with an increased solid phase stress, whilst the reference surface will depend on the hardening of the soil. The current stress point will always lie on the dynamic surface.

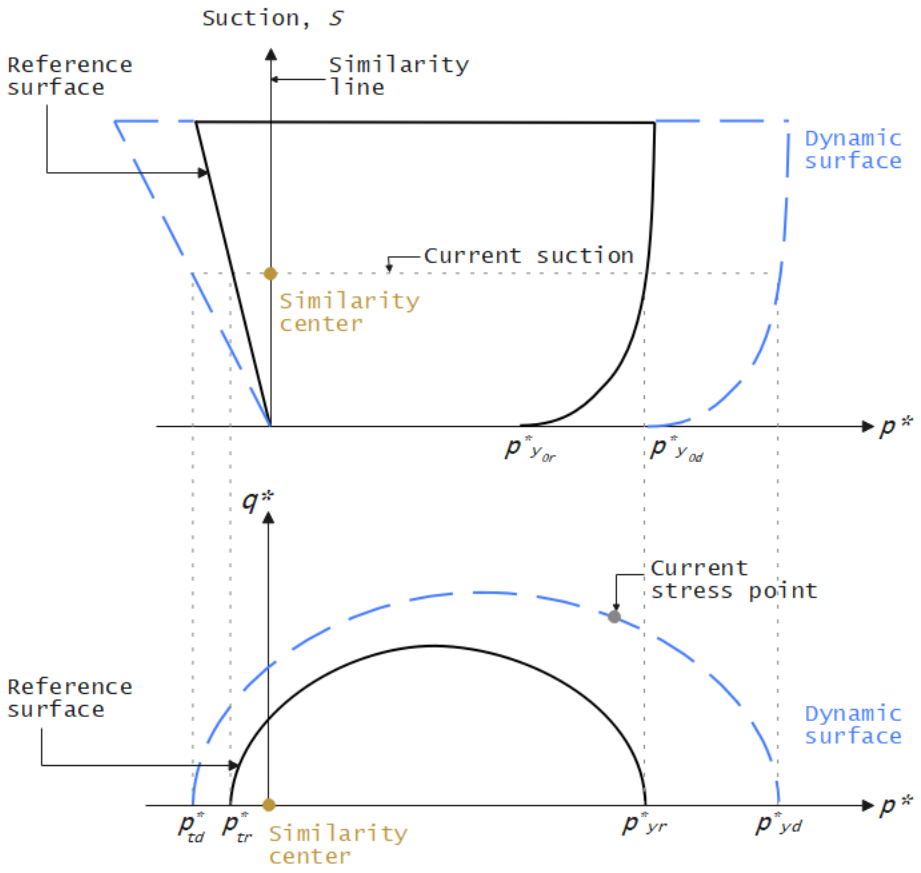

Figure 3.1: Illustration of the reference and dynamic surface in the $p^* - S$ and $p^* - q^*$ spaces. Adapted from Amiri et al. [2016a].

3.3.3 Hardening Rules

When the soil is exposed to plastic compression, the soil's behaviour will get stiffer. Therefore the reference surface will expand. However, plastic compression will also decrease the void volume, giving a lower segregation threshold value. A coupled hardening rule is used to capture this mechanism, where the grain segregation yield surface, given in Equation 3.17, will move downwards due to a lower segregation threshold value whilst the loading collapse reference surface expands. If ice segregation occurs, plastic dilation will happen. This will make the grain segregation yield surface move upwards whilst the reference surface will decrease, giving the soil a softer behaviour. The following equations provide the hardening rules to describe the two above phenomena.

$$\frac{\mathrm{d}p^*_{y0r}}{p^*_{y0r}} = \frac{1+e}{\lambda_0 - \kappa_0}\mathrm{d}\varepsilon_v^{mvp} + \frac{1+e}{\lambda_0 - \kappa_0}\mathrm{d}\varepsilon_v^{sp} \tag{3.18}$$

$$\frac{\mathrm{d}S_{seg}}{S_{seg} + p_{at}} = -\frac{1+e}{(\lambda_s + \kappa_s)}\left(1 - \frac{S}{S_{seg}}\right)\mathrm{d}\varepsilon_v^{mvp} - \frac{1+e}{s_w(\lambda_s + \kappa_s)}\mathrm{d}\varepsilon_v^{sp} \tag{3.19}$$

where λ_s denotes the compressibility coefficient for an increase in suction during the initial state. The amount of hardening is dependent on the unfrozen water content. The plastic resistance of the soil will increase with a decrease in water content. As stated in earlier research [Arenson et al., 2004], the shear strain will ruin the bonds between solid grains and ice, while increasing suction will make the bonds stronger. For the apparent cohesion of the soil, p^*_{tr}, the following hardening rule is therefore used

$$\frac{\mathrm{d}p^*_{tr}}{p^*_{tr}} = -k_{t_1}\frac{\mathrm{d}S}{p^*_{tr}}\left(H(-p^*_{tr}) \times H(\mathrm{d}S)\right) - k_{t_2} \cdot \mathrm{d}\varepsilon^{mvp}_q \tag{3.20}$$

where k_{t_1} and k_{t_2} are model parameters, whilst H is the Heaviside function given as

$$H(x) = \begin{cases} 0 & x \leq 0, \\ 1 & x > 0 \end{cases} \tag{3.21}$$

3.3.4 Flow Rules

The viscoplastic part of the strain increment coming from the variation of the solid phase stress, $d\varepsilon^{mvp}$, is calculated based on the similarity ratio by the following flow rule:

$$\mathrm{d}\varepsilon^{mvp} = \mu\left\langle R^N \right\rangle \frac{\partial Q_1}{\partial \sigma^*} \cdot \mathrm{d}t = \mathrm{d}\lambda_1 \times \frac{\partial Q_1}{\partial \sigma^*} \tag{3.22}$$

where $\langle\rangle$ is the Macaulay brackets, $\mathrm{d}t$ is the time increment, μ represents the fluidity of the system, N is often called the creep ratio and governs the rate sensitivity of the material. $\mathrm{d}\lambda_1$ depicts the plastic multiplayer regarding the loading collapse reference surface while Q_1 is the plastic potential function given as

$$Q_1 = \left[p^* - \frac{(1+\gamma s_i)p^*_{yd} + (1-\gamma s_i)p^*_{td}}{2}\right]^2 + \left(\frac{q^*}{M}\right)^2 \tag{3.23}$$

where γ is a material parameter. Whilst μ and N can be treated as constant parameters in unfrozen soils, the same is not the case for frozen soils. μ will depend on κ and λ, which will both vary with ice content, cryogenic suction and temperature. For the frozen state μ is therefore given as

$$\mu = \mu_0 \frac{\lambda - \kappa}{\lambda(\lambda_0 - \kappa_0)} \tag{3.24}$$

where μ_0 is the fluidity of the unfrozen state for the corresponding reference strain. As discussed in Section 2.3, the strain rate dependency will increase with an increasing ice content, s_i. Therefore N should decrease with an increasing ice content. Simultaneously, the rate dependency of ice will decrease with a decreasing temperature. Because of the temperature dependency, it is expected that N will increase with an increase in suction, S. This variation of N can be expressed as

$$N = N_0 + b_1 \times S - b_2 \times s_i \tag{3.25}$$

where N_0 is the strain rate coefficient of the unfrozen soil, whilst b_1 and b_2 represent two model parameters. Another flow rule is used to express the plastic part of the strain increment due to the suction variation. This is given as

$$\mathrm{d}\varepsilon^{sp} = -\mathrm{d}\lambda_2 \frac{\partial F}{\partial S}\mathbf{I} \tag{3.26}$$

where $\mathrm{d}\lambda_2$ depicts the plastic multiplayer due to the grain segregation yield surface. To determine the model parameters, both laboratory testing and numerical calibration must be done. Some parameters, such as the void ratio, the unit weight and the density of the soil can be determined by index testing, whilst other parameters require performance testing. Numerical calibration is used to determine model constants, such as the parameters b_1 and b_2 used when determining the suction and ice saturation dependency of N. This can, for instance, be done by performing triaxial or odometer tests on a relevant soil sample, and thereafter calibrating the model parameters to make the simulation as accurate as possible. More details about the determination of the parameters and numerical calibration are given in Chapter 5.

Chapter 4

Pile Loading Test at Longyearbyen

This master thesis is focused around an ongoing pile loading test in Longyearbyen, Svalbard; see Figure 4.1. In this chapter, an overview of the pile test and its preliminary results will be given. For the test, three wooden piles are placed on steel footing plates about 4.2 meters down in the ground, in the layer of marine permafrost. Sensors constantly measure the temperature and settlement at the bottom of the piles. In addition, the piles are incrementally loaded with concrete blocks to investigate the soil's settlement rate and creep behaviour. The loading test aims to study the time-dependent settlements with regard to temperature variation [Lyu et al., 2021b].

The research project is a part of the Nunataryuk project, founded by the European Union's Horizon 2020 Research and Innovation Program. The main purpose of the Nunataryuk project is to understand how thawing permafrost on land, along the coast and subsea can impact infrastructure, and indigenous and local communities in permafrost regions. And thereafter to develop targeted mitigation and adaption strategies for the identified challenges [Nunataryuk Project, 2021].

A field trip to Longyearbyen was carried out at the end of October 2022 to gather data from the pile loading test and to investigate the test set-up in order to model the ongoing test as realistically as possible.

4.1 Site Background

Longyearbyen is the largest settlement on Svalbard, with around 2000 inhabitants. In addition, many students and researchers are based in Longyearbyen, leading to increased human activity in the area. The town has a lot of infrastructure, such as bars, a supermarket, a church, a cinema, schools and a municipal swimming pool. Most of the infrastructure is founded on permafrost. Permafrost degradation can therefore impose a great risk to the integrity and stability of the present infrastructure. Longyearbyen is in need of more housing, and it is essential to build this sustainably with respect to climate change and the degradation of permafrost [Lyu, 2021].

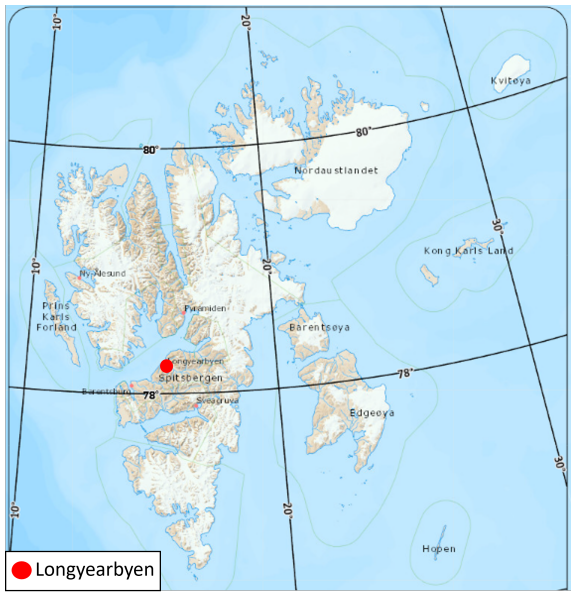

(a)

(b)

Figure 4.1: Overview of the pile test site. Figure (a) shows an overview of Svalbard, while Figure (b) shows an overview of the test site. Background maps are obtained from respectively Institute [2022b] and Institute [2022a].

Since 1980 the 30-year average air temperature has increased by 0.72 °C per decade in Longyearbyen [Instanes, 2016]. It is estimated that by 2100 the annual average temperature will increase by 4-6 °C, while the average winter temperature will increase by approximately 10 °C [Etzelmüller et al., 2011, Førland et al., 2011]. This will result in a degradation of the permafrost in the area. Field investigations from the pile test site show that the soil consists of two sand layers with a total thickness of approximately 3 meters on top of a marine clay layer. Overlying the permafrost in an active layer, approximately 2 meters thick, which is assumed to increase with time [Lyu et al., 2021c].

4.2 Experimental Setup of the Pile Loading Test

The foundation is designed to only resist the external loading by end bearing capacity. Therefore the piles are designed to minimise side friction. It should be noted that this is not standard practice for pile foundations in permafrost; however, in this project, the aim is not to design the most effective foundation but to study the bearing capacity and settlements concerning temperature variations and permafrost degradation. For this purpose, it is convenient to only look at end-bearing piles to limit the influencing parameters.

An illustration of the experimental setup is given in Figure 4.2. Three holes with a diameter of approximately 320 mm were predrilled for the piles. Thereafter about two liters of dry sand were placed at the bottom of the holes. A circular steel footing plate with a 280 mm diameter is attached to the bottom of the wooden pile. At the top of the pile, an equivalent 300 mm steel plate is attached.

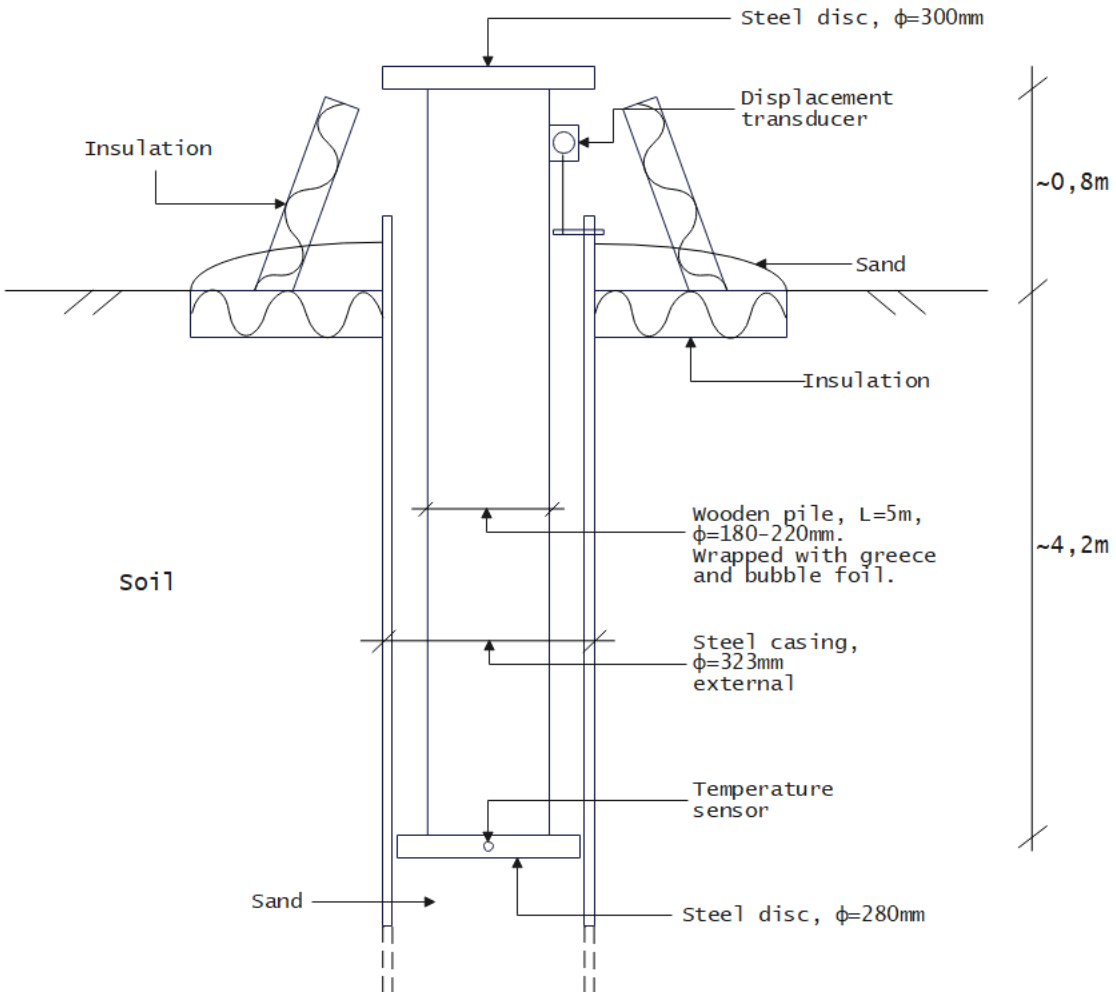

Figure 4.2: Illustrated profile of the pile loading test.

Steel casings are placed on the inside of the boreholes to support the soil and to provide an air gap along the shaft of the piles. This eliminates the contribution of side friction on the bearing capacity. The wooden piles are

waxed with grease and wrapped in bubble plastic to prevent ad-freeze bounds of water and ice. Thermal insulation is installed around the pile at the surface to decrease the heat exchange from air convection and to maintain the natural temperature conditions of the soil. Air convection is not a big problem during summer, as the warmer air will stay at the surface. However, in winter, cold air might flow down the air gap between the pile and casing, influencing the thermal regime.

A steel frame is constructed at the top of the pile, connecting the piles together and making a foundation for the added concrete slabs, ensuring an even distribution of the load. An overview of the pile loading test site is given in Figure 4.3. Load cells at the top of each pile measure the exact load the pile is subjected to. Vertical displacements are measured using a wire sensor placed between the wood pile and the steel casing, which is frozen to the soil beneath the pile. For reference measurements, an unloaded steel bar is fixed 5.5 m down in the ground, close to the three piles, as seen in Figure 4.3. The movements are also checked against the UNIS building nearby. Temperature sensors are placed at each footing plate. A small wind turbine and a solar panel have been installed to supply power to the logging of data during winter and summer.

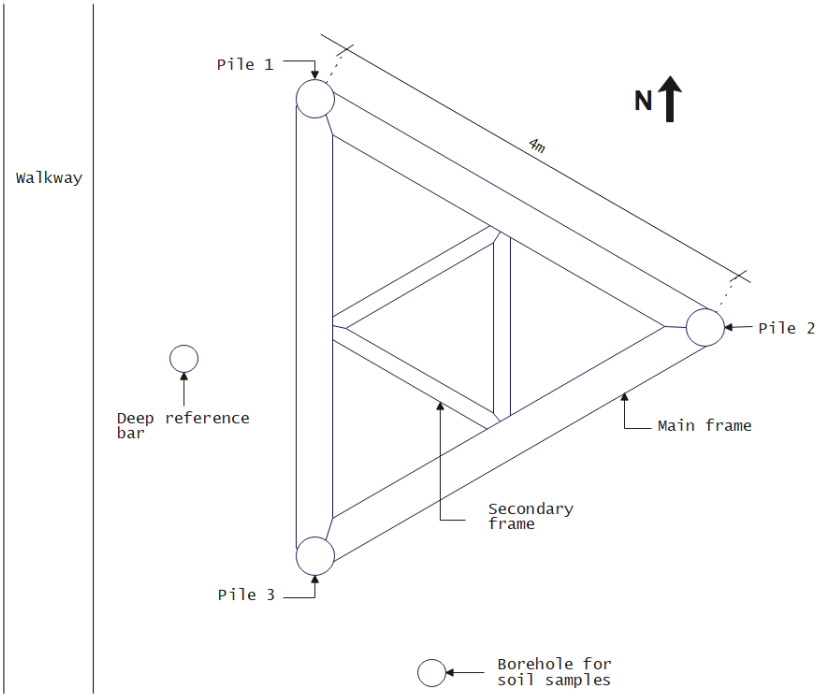

Figure 4.3: Illustrated overview of the pile loading test site

To get accurate results from the test, the soil should not be disturbed during the construction of the pile test set-up. Soils in permafrost are particularly sensitive to thermal disturbance. Due to this, sensor configurations were installed to monitor the soil temperature during construction. The construction was also conducted during late fall/winter, when the ground temperature was below zero degrees in the active layer, to reduce the impact of the construction phase. Wooden piles were favoured over steel due to lower thermal conductivity. A steel pile would, to a greater extent, be able to transport heat flow from the ground surface down to the bottom of the pile. A tent

shelter covers the top of the wooden piles to eliminate heat flow from the sun radiation, as seen in Figure 4.4. The set-up of the test began in April 2020. The test began in the middle of May 2020, loading two concrete slabs on top of the steel frame. Each concrete slab weighs 1400 kg. The step-wise load increased to 4, 6, 9 and 12 slabs in October 2020, March 2021, July 2021 and February 2022 respectively [Lyu et al., 2021b]. Pictures of the pile loading test after the last loading can be seen in Figure 4.4. In the picture the steel frame and concrete slabs are clearly shown. The wooden piles are hidden under the green tarpaulin, to eliminate heat flow.

(a) (b)

Figure 4.4: Pictures of the pile loading test after the last loading (12 concrete slabs).

In-situ samples were taken at a depth of 4-6 meters approximately 1 meter from the plate loading test. They have been tested to determine different mechanical and thermal properties, and the results are presented in Lyu [2021]. In addition, the results have been used to configure the numerical model for THM-simulations of the ground thermal regime and settlements, described in Chapter 5.

4.3 Preliminary Test Results from the Pile Loading Test

The ground temperature from the surface down to a depth of 30 meters has been measured by a thermistor close to the test site since the end of September 2018 in point E5, as shown in Figure 4.1. The measured surface temperature is presented in Figure 4.5, along with an estimated constant sinusoidal function for the surface temperature variation. The function is determined using a non-linear least square method to optimise the function to the temperature data. Unfortunately, the data sensor has had some measurement problems, resulting in periods with fewer measurements, especially in 2021, as seen in the figure.

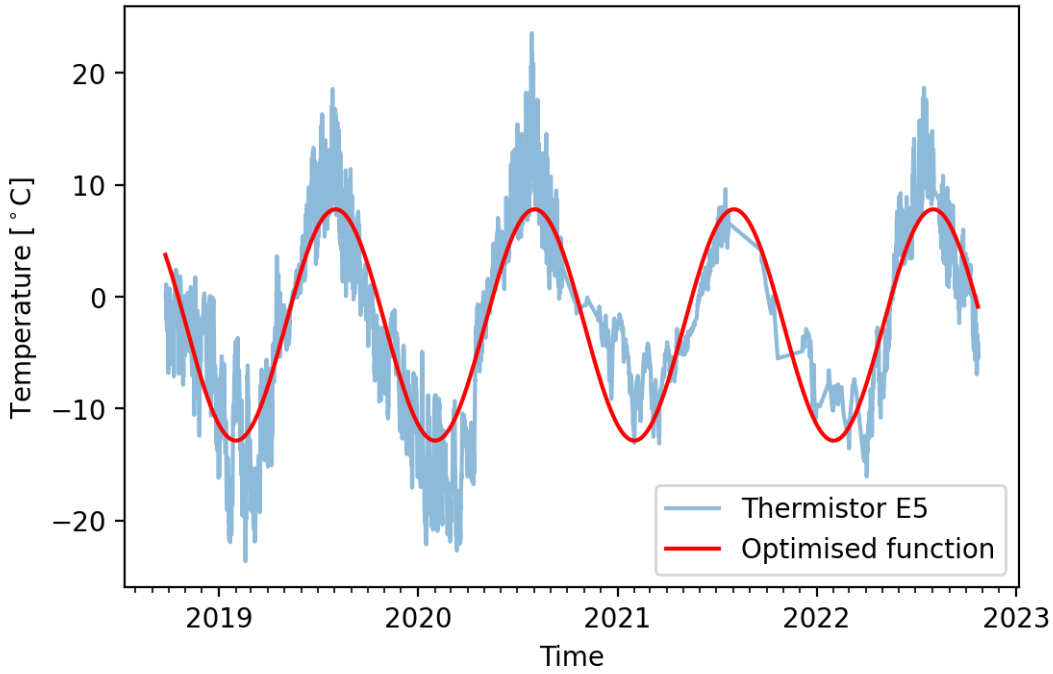

Figure 4.5: Measured surface temperature of thermistor E5 along with an optimised sinusoidal function of the temperature.

Calibrated thermistors have measured the temperature at the three pile tips since the beginning of August 2020. Another set of sensors were installed in May 2020, but these were not appropriately calibrated. The settlement of the piles has been logged since May 2020, but only data from August 2020 and onwards has been obtained. The results are shown in Figure 4.6. From the figure, one can see last winter was colder than the one before it, giving a lower minimum temperature. Furthermore, one can see the delay in temperature fluctuations from the surface to the pile tip, as described in Section 2.1, by the difference in Figure 4.5 and Figure 4.6. The surface temperature has a maximum and minimum in July and February, respectively, while the pile tip temperature has a maximum and minimum in February and May/June, respectively.

From Figure 4.6, one can see that when the external load is increased, implied by black arrows in the figure, an immediate increase in the pile tip displacement follows. Furthermore, one can see that whenever the temperature is approaching the maximum, around -3 °C, the creep rate increases, which happens around December each year. This is in accordance with the theory given in Section 2.3.3. One can see how the creep rate is approximately constant and then changes to a new, almost constant rate when the temperature approaches -3 °C.

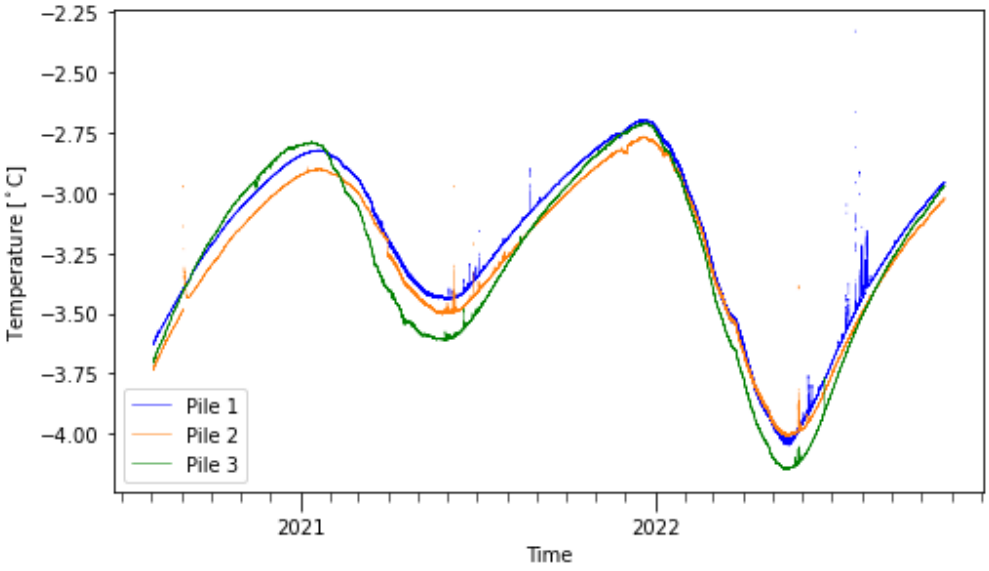

(a) Ground temperature at pile tip

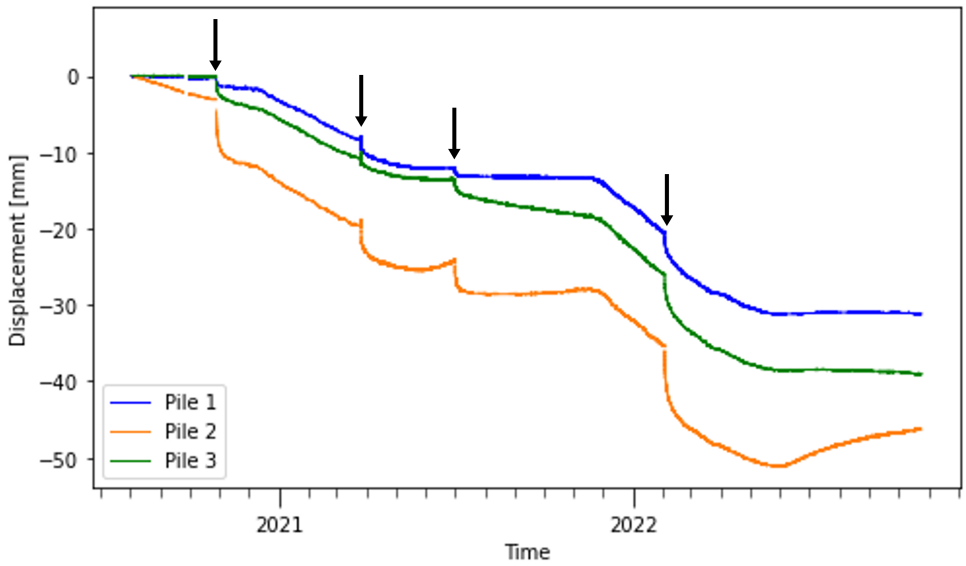

(b) Displacement at pile tip

Figure 4.6: Measurements from each of the piles.

The thawing/freezing temperature of the clay layer is approximately -1.6 °C due to its salt content. Still, as stated in Section 2.3, there will be transitions between the solid and liquid water phases at lower temperatures, as there is no definite distinction between the two phases. The unfrozen water content will rapidly increase when the soil temperature rises towards the thawing temperature. This can lead to an increase in creep rate and primary consolidation. When the unfrozen water saturation increases, the ice content will decrease, resulting in a higher load pressure on the remaining ice and therefore a higher creep rate. An increase in unfrozen water content can also lead to an increase in consolidation. Normally the impact of consolidation on the total settlements is low in frozen soils. Still, as the unfrozen water content increases, the effect can be significant, as mentioned in Section

2.3.3. Therefore, it should not be ruled out that consolidation may have an impact on the increased settlement rate observed around December each year.

Figure 4.6 also shows how Pile 2 has a bigger displacement than the two other piles. Even though the piles are placed close together, within 4 meters of one another, the soil properties may vary. A soil will never be wholly homogeneous, and local differences should be expected. Therefore it is natural that the displacement varies to some degree, as is witnessed in Figure 4.6. However, the big difference in instant displacement after the second loading (October 28th 2020) might indicate a measuring error for Pile 2. From Figure 4.6, one can also see that the displacement of Pile 2 decreases from around June 2022. This could be due to the accumulation of ice lenses under the pile tip. However, it is uncommon for ice lenses to form in the permafrost layer. Instead, they normally form in the freezing zone in the active layer, as described in Section 2.2.2. Due to the deviations of Pile 2, the main focus should be placed on the measured settlements from Pile 1 and 3.

Chapter 5

Numerical Modelling of the Pile Loading Test

It has been carried out simulations of the pile loading test described in Chapter 4 using the elasto-viscoplastic model described in Chapter 3. The simulations aim to investigate if the model can represent the behaviour of the frozen soil with an acceptable level of accuracy. This chapter concerns the determination of model parameters and the numerical setup, whilst the results from the simulations are presented in Chapter 6. The calibration of the model parameters and simulations of the frozen soil are carried out in PLAXIS 2D, version V21.1, which is a commercially available two-dimensional finite element program.

5.1 Previous Analysis

As mentioned in Section 3.1, the behaviour of frozen soils can be modelled using THM (Thermo-Hydro-Mechanical) simulations. However, a thorough job must be done with the parameter determination and the numerical scheme calibration in order to obtain acceptable results. The elastic-viscoplastic model used in this thesis contains around 30 parameters and it is thus inevitable that a large effort is required to determine all the parameters. Typically the model parameters are determined using a trial and error method which aims to calibrate the numerical simulations with experimental results. The experimental tests should preferably be of samples taken at the relevant area. As mentioned in Section 1.1, the pile loading test in Longyearbyen has already been researched in the PhD dissertation Lyu [2021], where both laboratory tests and numerical simulations are presented. For the model setup given in this thesis, the information from this dissertation has been used as a basis and thereafter modified and calibrated to attain good accuracy. Permafrost soil samples of the marine soil 1 m from the pile test at a depth of 4-6 meters were collected, and laboratory tests such as the measurement of the unfrozen water content and undrained shear and creep tests were carried out. The results are presented in the dissertation. Furthermore, undrained triaxial creep tests were done at two different temperatures and with varying deviatoric stress, q. The model parameters for the

elasto-viscoplastic model were calibrated with the experimental results of these tests. Both the parameters and the experimental results are given in Lyu et al. [2021c]. Due to upgrades in the newer versions of PLAXIS 2D and lack of information on some of the settings and parameters, using the exact parameters from Lyu et al. [2021c] will not give the same results as achieved in the dissertation. Therefore, a new calibration is necessary to achieve a proper fit between the triaxial creep results and the equivalent simulations in PLAXIS 2D V21.1. The properties of the samples used for triaxial creep tests can be found in Table 5.1. The test was conducted at two different temperatures: -3 and -5 °C with a varying deviatoric stress, q. From the table, one can see that the depth of the samples differs slightly and can affect the correlation between the laboratory tests and the simulations to some degree.

Table 5.1: Properties of the samples used for triaxial creep tests done by Lyu [2021].

Test no.	**Depth [m]**	**T [°C]**	**S [g/L]**	**wc [%]**	σ_3 **[kPa]**	**q [kPa]**
1	4.2~ 4.6	-3	24	22.3	100	191
2	4.2~ 4.6	-3	26	22.0	100	248
3	4.2~ 4.6	-3	25	22.2	100	345
4	4.6~ 5.0	-3	27	20.9	100	450
5	4.6~ 5.0	-5	24	19.5	100	273
6	4.6~ 5.0	-5	25	20.2	100	364
7	4.6~ 5.0	-5	24	19.9	100	490
8	4.6~ 5.0	-5	25	23.0	100	558
9	4.2~ 4.6	-5	21	21.9	100	728
10	4.6~ 5.0	-5	30	20.0	100	1450

T: temperature, S:salinity, wc: gravimetric water content, σ_3: cell pressure, q: deviatoric stress.

5.2 Numerical Calibration of Model Parameters

Firstly the parameters given in Lyu et al. [2021c] were implemented for the soil material. Subsequently, simulations of undrained triaxial creep tests were done. As explained in the previous paragraph, results did not coincide entirely with the simulated results in Lyu et al. [2021c], and a new calibration is therefore necessary to improve the results. For simulating the triaxial creep tests, the PLAXIS 2D Soil test was used with the test settings given in Figure 5.1. For Phase 1, the vertical stress is increased. Subsequently, the stress is held constant in Phase 2 to simulate the creep behaviour after loading. The deviatoric stress, q, varies for each sample and is given in Table 5.1. It should be noted that the triaxial simulations are sensitive concerning the number of steps in each phase. Therefore the same ratio of 10 seconds per step has been used for all the simulated samples to be able to compare the results.

Initial		Initial stresses	Boundary condi...	
	σ_{xx}	-1E005 N/m²	Stress inc XX	
	σ_{yy}	-1E005 N/m²	Stress inc YY	
	σ_{zz}	-1E005 N/m²	Stress inc ZZ	
	τ_{xy}	0 N/m²	Strain inc XY	
Phase 1			**Increments**	
Duration	1000 s	$\Delta\sigma_{xx}$	0	N/m²
Steps	100	$\Delta\sigma_{yy}$	-3E005	N/m²
		$\Delta\sigma_{zz}$	0	N/m²
		$\Delta\gamma_{xy}$	0	%
Phase 2			**Increments**	
Duration	1E005 s	$\Delta\sigma_{xx}$	0	N/m²
Steps	10000	$\Delta\sigma_{yy}$	0	N/m²
		$\Delta\sigma_{zz}$	0	N/m²
		$\Delta\gamma_{xy}$	0	%

Figure 5.1: Settings for simulations of undrained triaxial creep test. The duration and number of steps for phase 2 and the increment of $\Delta\sigma_{yy}$ = q varies for the different tests.

The tests done at -3°C showed a higher sensitivity with regards to the given freezing temperature than the tests done at -5°C. In general, a change in the given freezing temperature will have a greater impact the closer the freezing temperature is to the tests that are done. For a better correlation between the simulations and laboratory tests, the freezing temperature, T_f, was changed from 271.60 K (-1.55 °C) to 271.70 K (-1.65 °C). This gave a significant change in the results at -3°C while the results at -5°C were approximately the same. Another important parameter in the model is N, often called the creep ratio. As described in Section 3.3, the parameter can be expressed as a function of the cryogenic suction, S, and the ice content, s_i. It is given by equation (3.25), replicated below

$$N = N_0 + b_1 \times S - b_2 \times s_i$$

where N_0, b_1 and b_2 are numerical constants that must be decided. The viscoplastic part of the strain increment from the solid phase stress, given in Equation (3.22), is calculated with a term of the equation raised to the power of N. Because of this, the calculated strain is very sensitive to the value of N. A small change in the input parameters describing N can therefore significantly change the strain results. It is difficult to determine the function of N directly from laboratory tests. However, N can be estimated by setting b_1 and b_2 to zero and finding a value of $N = N_0$ that gives a good correlation between the simulations and experimental results for each of the test temperatures: -3 °C and -5 °C. To determine N_0, b_1 and b_2, the cryogenic suction, S, and ice saturation, s_i, given in Equation 2.3, 5.1 and 5.2 was calculated at both -3°C and -5°C. Thereafter, a back-calculation was done to determine the values of N_0, b_1 and b_2, giving sufficient accuracy at both temperatures.

$$S = p_i - p_w = \rho_i l \ln \frac{T}{T_0} \tag{2.3}$$

$$s_i = 1 - s_w \tag{5.1}$$

$$s_w = \left[1 + \left(\frac{p_i - p_w}{p_r}\right)^{\frac{1}{1-\lambda_r}}\right]^{-\lambda_r} = \left[1 + \left(\frac{S}{p_r}\right)^{\frac{1}{1-\lambda_r}}\right]^{-\lambda_r} \tag{5.2}$$

The results of the back calculations are shown in Table 5.2, where the given values for N_0, b_1 and b_2 are used later on for the simulations. The measured temperature at the pile tip, given in Figure 4.6a, shows that the temperature varies between -4 to -2.5 °C. Therefore the tests done at -3 °C are prioritised in the numerical calibration, as they are in the relevant temperature range. This explains why there is a bigger deviation between the target value and the calculated value of N for T=-5 °C.

Table 5.2: Calibrated N

	T=-3°C	**T=-5°C**
N_{target}	13.5	15.0
s_i	16.55%	32.57%
S	1.752 Mpa	4.028 Mpa
$N_{calculated}$	13.50	14.79
N_0	22	
b_1	1.64E-5	
b_2	225	

In Figure 5.2 and Figure 5.3, the results of the simulations for the triaxial creep tests before and after calibration of N are given, along with the experimental results of the triaxial creep tests.

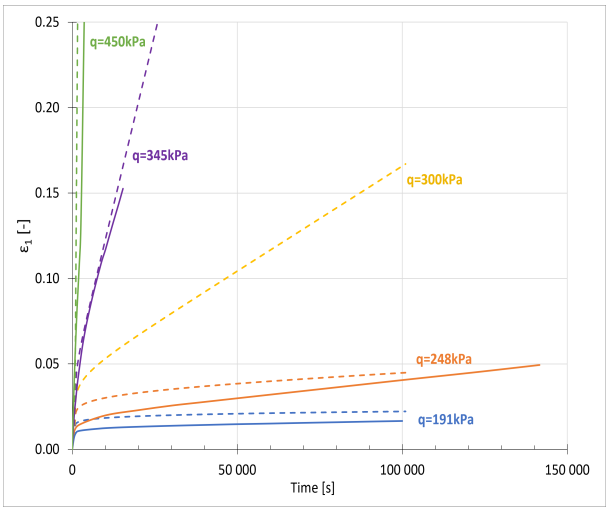

(a) Before calibration

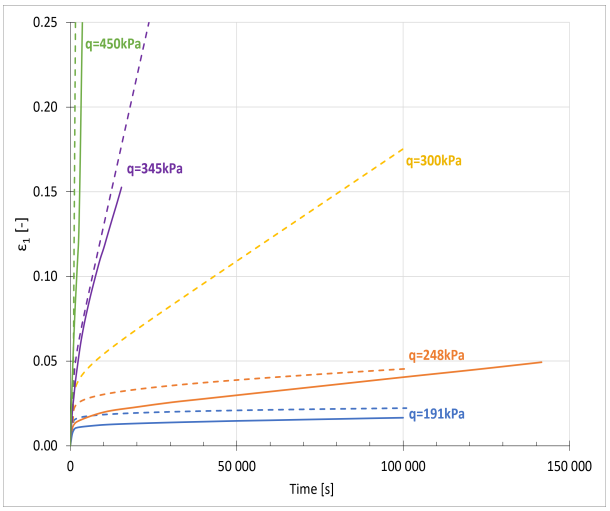

(b) After calibration

Figure 5.2: Calibration of the strain rate coefficient for the triaxial tests at -3°C. Dashed lines show simulated results, whilst full lines show the laboratory results.

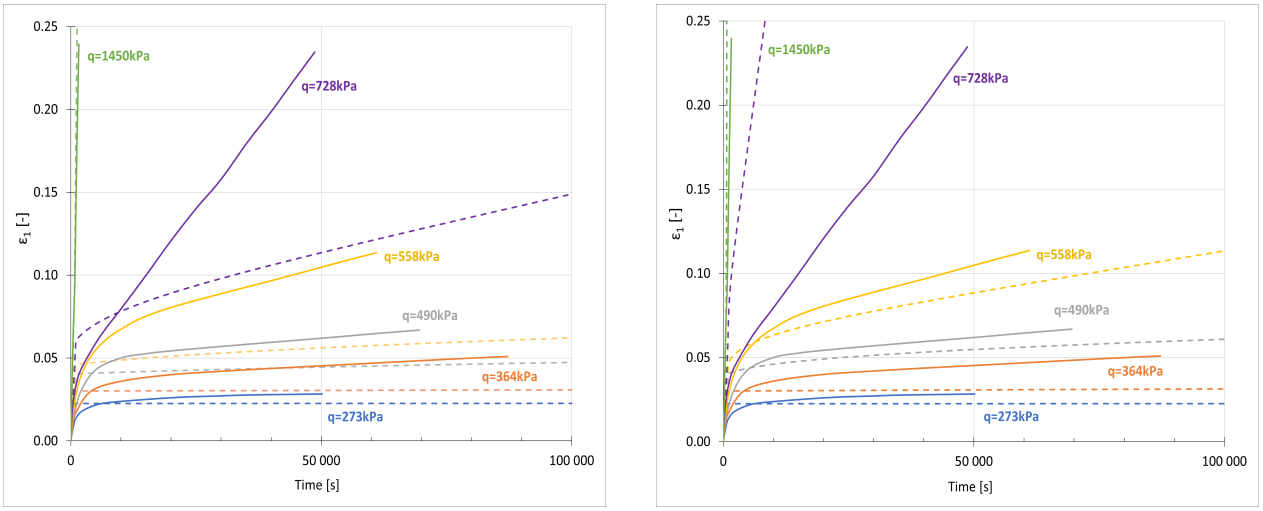

(a) Before calibration

(b) After calibration

Figure 5.3: Calibration of the strain rate coefficient for the triaxial tests at -5°C. Dashed lines show the simulated results, whilst full lines show the laboratory results.

As mentioned in Section 2.3.3 the creep deformation rate is assumed to increase with increasing temperature for frozen soils, which also can be seen from Figure 5.2 and Figure 5.3. From the figures, one can see that the tests done at -3 °C has a softer behaviour than those done at -5 °C, as the time-dependent strain is higher for similar values of deviatoric stress, q. This corresponds to a higher creep rate deformation for the samples done at -3 °C. From Figure 5.2, one can see that the results for -3 °C are very similar before and after calibration. Figure 5.3 shows that there is a more significant difference for -5 °C. The results are approximately the same as before calibration for q=263, q=364, and q_{max}= 1450 kPa. For q=490 and q=558 kPa, the results after calibration have a much lower deviation. However, one can see that for sample 7, q=728 kPa, the results after calibration have a significant deviation from the results before calibration. It should be mentioned that the soil sample tested for q=728 kPa is from a different depth than the other samples for -5 °C, as shown in Table 5.1. The results after calibration show a too-soft behaviour for the sample, whilst the results before calibration have a too-stiff behaviour. Logically one should expect that the model is showing a too-stiff behaviour, as in Figure 5.3a, as the sample is from a smaller depth than the other samples. Overestimating the depth of a sample should result in an increased strength and a too-stiff behaviour due to a higher in-situ stress-state, given a homogeneous soil. A reason for the deviation might be a variation in the mechanical properties of the samples, such as a stronger shearing strength in sample number 7. In general, the calibration is very sensitive for changes around $q = \frac{1}{2}q_{max}$. Consequently, a slight change in input parameters, such as N_0 or the freezing temperature, T_f, can greatly impact the inclination of the slope. This is evident for sample 7, q=728 kPa, in Figure 5.3, where there is a significant change in slope inclination before and after the calibration.

5.3 Final Model Parameters

A soil will never be perfectly homogeneous, and it is therefore impossible to get a perfect correlation for all the samples, as the properties will vary throughout the soil layer. Therefore, the aim is to optimise the set of parameters to get the best results possible for the totality of the samples. The final parameters used in the simulation of the pile loading test are given in Table 5.4 and Table 5.3. The sand layers at the top of the geometric model are assumed to be perfectly elastic materials due to the lack of experimental results and to simplify the numerical calculation. This assumption should have a negligible effect on the simulation results [Lyu et al., 2021c], as the pile footings are installed in the marine clay layer. In addition to the freezing temperature, T_f, and the strain rate coefficient, N, some other parameters have also been changed from the values given in Lyu et al. [2021c]. The reference coordinate for p^*_{y0r}, Y_{ref} and the rate of change in p^*_{y0r}, Δp^*_{y0r} have also been changed, to avoid an unrealistic creep settlement of the soil. All model parameters with modified values are marked with grey in Table 5.4.

Table 5.3: Parameters of the two sand layers

Parameter	**Description**	**Unit**	**Sand 1**	**Sand 2**
e	Void ratio	-	0.270	0.351
ρ_s	Solid density of the soil	kg/m^3	2000	2700
λ_{s1}	Thermal conductivity	W/(m·K)	1	4
c_s	Specific heat capacity	J/(kg·K)	1250	
λ_r	Parameter for fitting unfrozen water saturation curve	-	0.5	
ρ_r	Parameter for fitting unfrozen water saturation curve	Pa	1E5	
T_f	Freezing/melting temperature	K	272.65	
E'	Young's modulus	Pa	30E6	
ν	Poisson's ratio	-	0.3	
k	Permeability	m/s	1	

Table 5.4: Parameters of the marine clay layer

Parameter	Description	Unit	Value
T_{ref}	Reference temperature	K	273.16
E_{fRef}	Frozen soil Young's modulus at T_{ref}	Pa	1E6
E_{fIncr}	Rate of change in Young's modulus with temperature	Pa/K	1E6
ν_f	Frozen soil Poisson's ratio	-	0.47
G_0	Unfrozen soil shear modulus	Pa	5E6
κ_0	Unfrozen soil elastic compressibility coefficient	-	0.01
P_c^*	Reference stress	Pa	-10000
λ_0	Elastic-plastic compressibility coefficient for unfrozen state	-	0.05
γ	Plastic potential parameter	-	1
K_{t1}	Rate of change in apparent cohesion with suction	-	0.11
M	Slope of the critical state line	-	1.2
λ_s	Elastic-plastic compressibility coefficient for suction variation	-	0.004
κ_s	Elastic compressibility coefficient for suction variation	-	8E-5
r	Coefficient related to maximum soil stiffness	-	0.1
β	Rate of change in soil stiffness with suction	Pa^{-1}	5E-8
λ_r	Parameter for fitting unfrozen water saturation curve	-	0.3
ρ_r	Parameter for fitting unfrozen water saturation curve	Pa	2E6
α	Parameter for the pressure dependency of ice thawing temperature	-	9
T_f	Freezing/melting temperature	K	271.60
p_{ref}	Parameter for the pressure dependency of ice thawing temperature	Pa	-395E6
m	Yield parameter	-	1
K_{t2}	Hardening parameter for apparent cohesion	-	0
μ_0	Fluidity parameter for unfrozen state	s^{-1}	5E-9
N_0	Rate dependency parameter for unfrozen state	-	15.2
b_1	Rate of change in N with suction	Pa^{-1}	6.1E-6
b_2	Rate of change in N with ice saturation	-	74.9
p_{y0r}^*	Initial reference preconsolidation stress for unfrozen state	Pa/m	-40000
Y_{ref}	Reference coordinate for p_{y0r}^*	m	-4
Δp_{y0r}^*	Rate of change in p_{y0r}^*	Pa	-10000
$S_{s,seg}$	Initial segregation threshold	Pa	1.5E9
e	Void ratio	-	0.621
ρ_s	Solid density of the soil	kg/m^3	2700
λ_{s1}	Thermal conductivity	W/(m·K)	2.6
c_s	Specific heat capacity	J/(kg·K)	1250

Listed in the order given in PLAXIS V21.1.

5.4 PLAXIS 2D; Model Setup

The soil is modelled with two sand layers followed by a marine clay layer. An illustration of the geometry of the simulation domain is given in Figure 5.4. Screenshots showing the soil polygon, calculation phases and model settings in PLAXIS can be found in Appendix 8.2. The setup can be defined as a boundary value problem, solved using the finite element method. An axisymmetric soil polygon is used, meaning the polygon is symmetric around the y-axis, seen in Figure 5.4. The soil polygon consists of 1115 elements and 9135 nodes. The element mesh is automatically generated by PLAXIS, but has been refined around the pile tip, giving four elements over the pile radius. In general, the mesh is finer around the pile, and more coarse further from the pile. A finer mesh can give

more accurate results, but will also increase the computation time. For this model, a finer mesh was tested but did not affect the results in a noteworthy way. In contrast, the mesh could have been coarser in most of the model. However, due to the initial temperature condition, explained further down in Section 5.4.1, it was not possible to make the mesh much coarser, as each depth with an assigned initial temperature will act as a dividing line between soil elements.

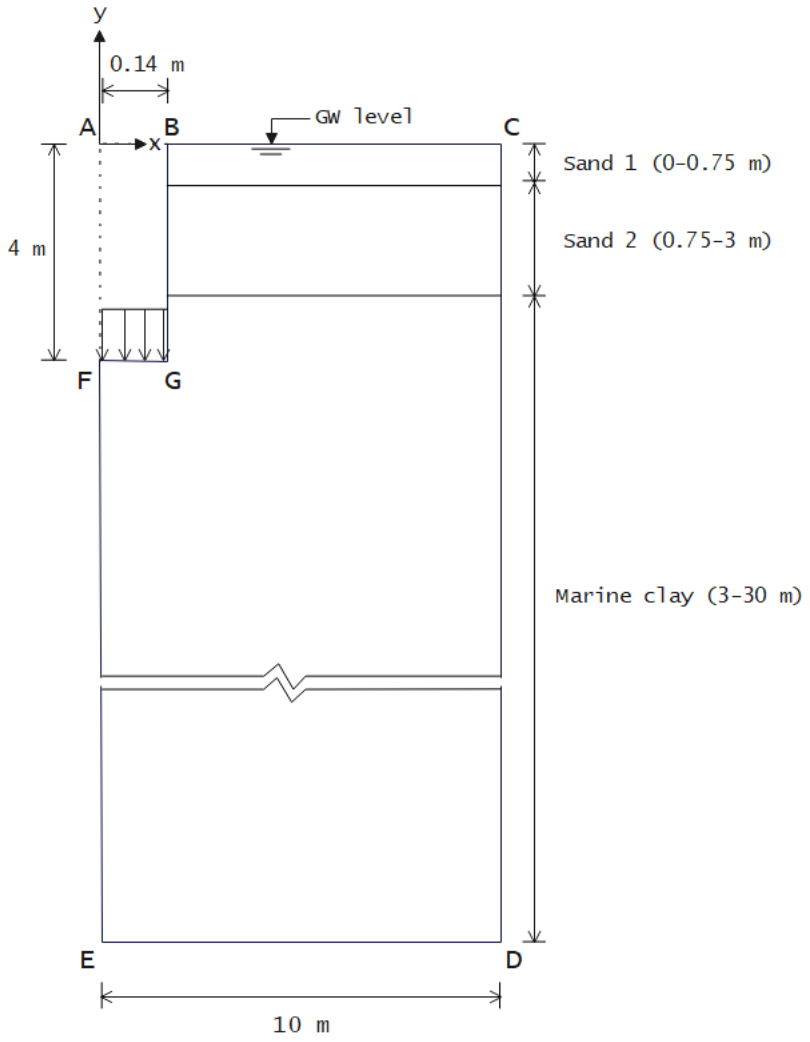

Figure 5.4: An illustration of the soil polygon. Adapted from [Lyu, 2021].

Table 5.5 shows the time periods of the different loading steps and the equivalent load on each pile tip, including the load from the wooden piles and steel frame.

Table 5.5: Loading dates and quantities

Startdate	Enddate	No. Concrete Slabs	Load per Pile [kPa]	No. Days
14.05.2020	28.10.2020	2	227	166
28.10.2020	26.03.2021	4	387	148
26.03.2021	01.07.2021	6	546	96
01.07.2021	02.02.2022	9	784	215
02.02.2022	24.10.2022	12	1 023	263

The unfrozen water content for the marine clay layer is calculated by the elastic-viscoplastic model used. For the sand layers, which are modelled as elastic layers, a function for the unfrozen water content has been implemented, as shown in Figure 5.5. The curve is approximated by the UWS (Unfrozen Water Saturation) function in [Lyu et al., 2021a], based upon the assumption that the sand is non-saline and coarse-grained with a freezing temperature of -0.5 °C, as stated in a NGTS (Norwegian Geo-Test Sites) report describing the permafrost conditions in the area of the pile test site [Gilbert et al., 2019].

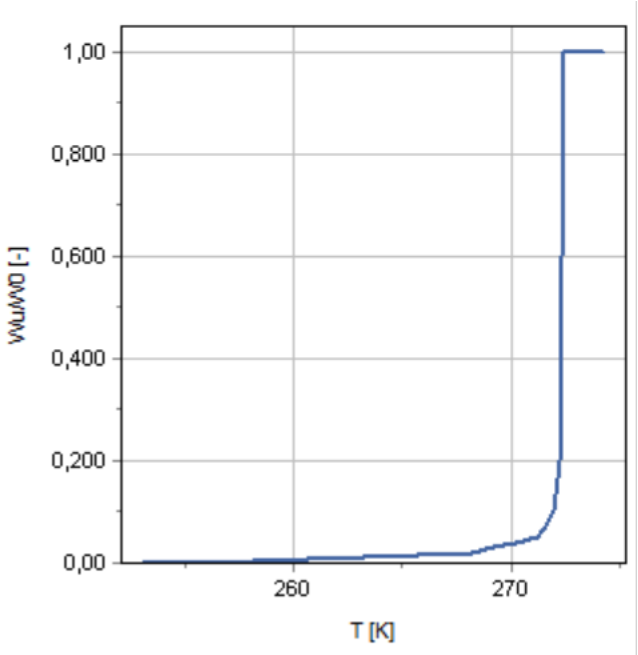

Figure 5.5: Function of the unfrozen water content (WU/W0) with respect to temperature for the sand layers.

For the clay layer, the elasto-viscoplastic model described in Chapter 3 is used. As explained in Section 3.3, this model uses the definition of solid phase stress given by Equation 3.1, and not the effective stress in its formulation. However, the PLAXIS software will by default use Terzaghi's effective stress definition. To ensure that the solid phase stress is used for the clay layer and not the effective stress, it is important to use fully coupled flow-deformation as the calculation type for all the calculation phases in PLAXIS, except the initial phase. A fully coupled

flow-deformation will simultaneously analyse the development of deformations and pore pressures due to time-dependent changes in the hydraulic boundary conditions. Combining the fully coupled flow-deformation with temperature calculations allows for a THM-analysis (Thermo-Hydro-Mechanical), which is essential in simulating the behaviour of frozen soils. The THM-analysis will simultaneously account for how time-dependent temperature changes will affect stress, deformation and groundwater flow in the soil [Bentley, 2021].

The hydraulic conductivity of the unfrozen soil has not been measured and is assumed to have a constant value of $k = 0.001$ m/s for all layers. Furthermore, it is assumed that the relative hydraulic conductivity, k_r, follows the van Genuchten function, given as:

$$k_r = \sqrt{S_w}\left[1 - \left(1 - S_w^{1/\lambda}\right)^{\lambda}\right]^2 \tag{5.3}$$

and that this is valid for all frozen soils with fully drained boundary conditions. The parameter governs water flow through the material. The van Genutchen function is originally meant for unsaturated soils, where the pore volume is filled with air and water. However, it can also work for saturated frozen soil, where the pore volume is filled with liquid water and solid ice. The water saturation is then given as $s_w = 1 - s_i$, as stated earlier in Section 3.3.

5.4.1 Boundary conditions

For the top boundary (AC on Figure 5.4), an optimised sinusoidal function, based on the measured ground surface temperature from thermistor E5, shown in Figure 4.5, is used. For the bottom boundary (DE), an upward geothermal heat flux of 65 mW/m^2 is applied, as suggested by Etzelmüller et al. [2011] and used in [Lyu, 2021]. All other boundaries are thermally insulated (closed). The hydraulic boundaries are set to be hydraulically conductive (allow seepage), except the axisymmetric axis (EF), FG and GB, which are closed. The bottom boundary (DE) is mechanically fixed, whilst the other boundaries are horizontally fixed but can deform vertically.

There is a delay between the surface temperature and the corresponding ground temperature because of the thermal diffusivity, as explained in Section 2.1. Because of this, an initial temperature distribution through the soil is necessary when the calculations start. As mentioned in Section 4.3, the calibrated temperature sensors started logging data about three months after the pile loading test began. Therefore the measured temperature-depth distribution from the nearby thermistor E5 has been used as the initial condition. The temperature-depth distribution is shown in Figure 5.6, and is taken from the first day of loading.

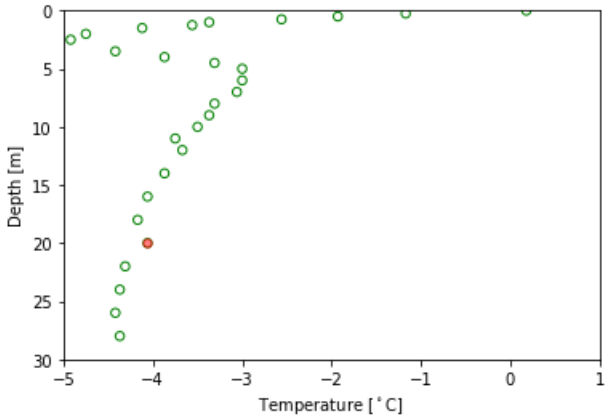

Figure 5.6: Profile of the ground temperature at thermistor E5 on the first day of loading. The red point has been disregarded.

Every point has been added as a constant temperature initial condition through the soil for the first calculation phases until the loading starts. For the point marked red in Figure 5.6, a correction has been done to avoid a deviation from the rest of the curve. If a ground temperature distribution is unavailable, another solution would be to let the model run with a surface temperature boundary condition for a while to calibrate a ground thermal regime before simulating the excavation and loading.

Chapter 6

Analysis and Results

This chapter presents and discusses the results from the PLAXIS simulation described in Chapter 5. For additional information regarding the simulation results and model settings in PLAXIS, see Appendix 8.2. The most significant results to analyse are the temperature and displacements at the pile tip, as these results can be compared to the corresponding experimental data presented in Section 4.3. The PLAXIS model is run for the time period from the first loading on the 14th of May 2020 until the 24th of October 2022, which is the last day with gathered experimental data. The dates of each loading phase can be seen in Table 5.5. The computation time for the simulation was approximately 2 hours, using a processor with a speed of 2.80 GHz and an installed RAM (Random Access Memory) of 128 GB.

6.1 Simulated Settlements

Figure 6.1 shows the simulated footing settlement at the pile tip along with the measured settlement at each pile tip. While the simulation began at the first loading in May 2020, experimental data has only been obtained from the beginning of August 2020 and onwards. This can be seen in the presented figures showing the comparison between the numerical simulations and the experimental data. For Figure 6.1 and Figure 6.2, showing the comparison of settlements, the experimental data is fitted to the simulated curve at the beginning of logging (August 2020). The immediate settlement from the first loading in May 2020 has therefore not been measured, and a possible deviation between the simulated and the actual settlements from May to August 2020 is not shown in the figures.

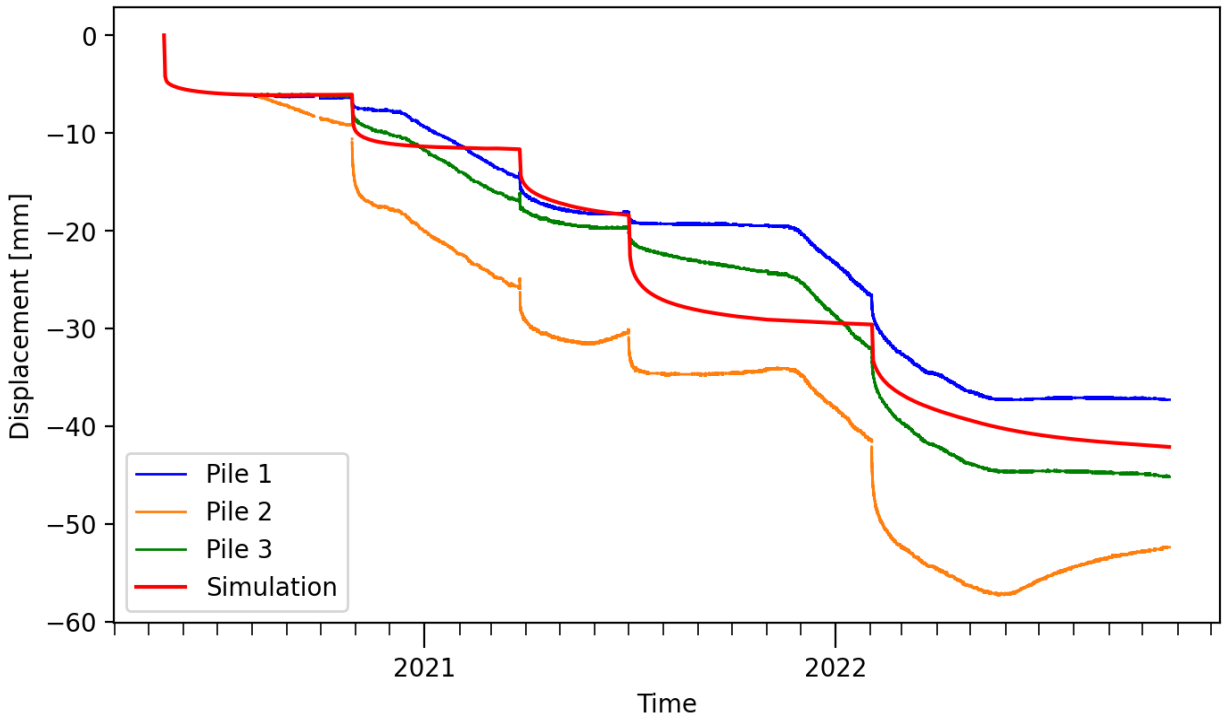

Figure 6.1: Model simulation of the settlements at the pile foot along with data loggers of the settlement at each pile foot.

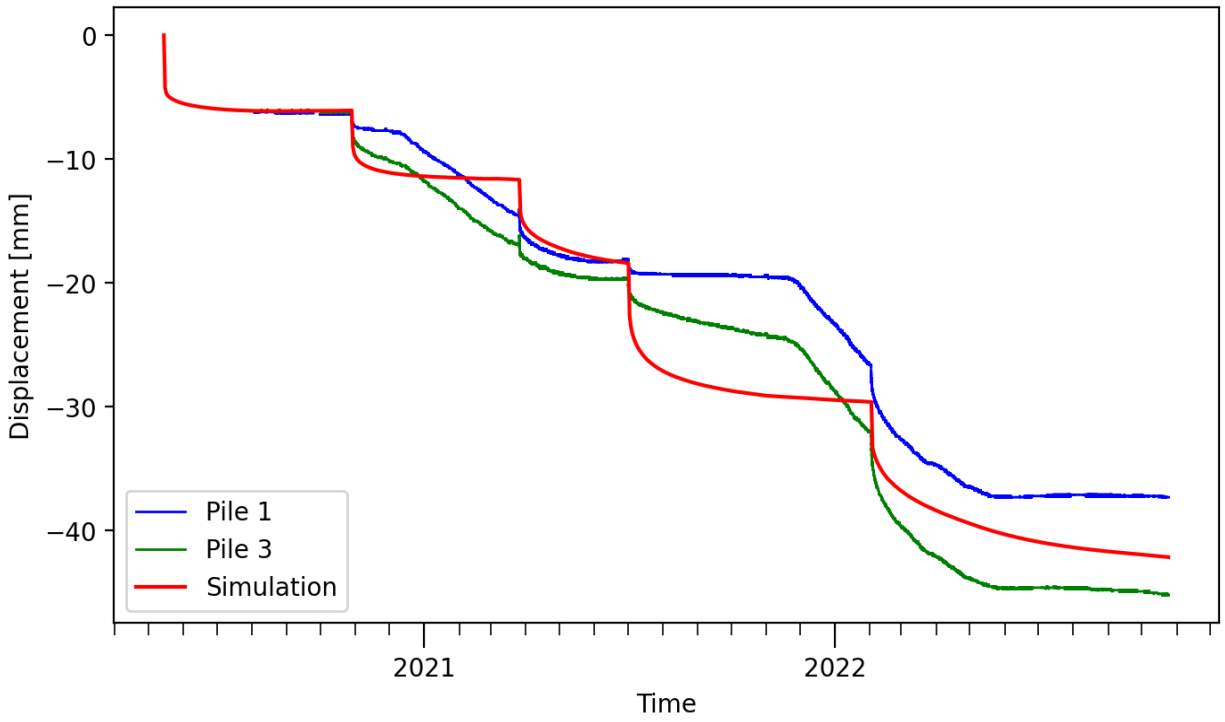

Figure 6.2: Model simulation of the settlements at the pile foot along with data measurements from Pile 1 and Pile 3.

The simulated settlements are of the same magnitude as the measured settlements, as seen in Figure 6.1. The simulated settlement coincides best with the measured settlements from Pile 1 and 3. As discussed in Chapter 4, the creep rate increases whenever the ground temperature approaches -3 °C, as seen around December each year. The model does not produce this change in creep deformation rate, as illustrated in Figure 6.2, which shows the comparison of the simulated settlements and the measured settlements from Pile 1 and 3. Here one can see that the immediate settlement after loading is bigger for the model, whilst the creep settlement is a lot lower. immediate settlements heavily dominate the simulation, especially for the first two loading steps shown in Figure 6.3, whereby the creep settlements can almost be neglected. As the immediate settlement is overestimated and the creep settlement is underestimated, the total settlements at the end of the measured time period coincide very well with Pile 1 and 3. Possible reasons for the deviation in settlements are further discussed in Chapter 7.

In Figure 6.3, the simulated settlement is presented, where each loading is illustrated with a black arrow and the added number of concrete slabs. From the figure, one can see a big immediate settlement after every loading. The immediate settlements do not increase significantly with each loading step. Figure 6.3 shows that the immediate settlement of the first loading is greater than that of the second and third loading. The creep settlements however, seem to be increasing with each loading step.

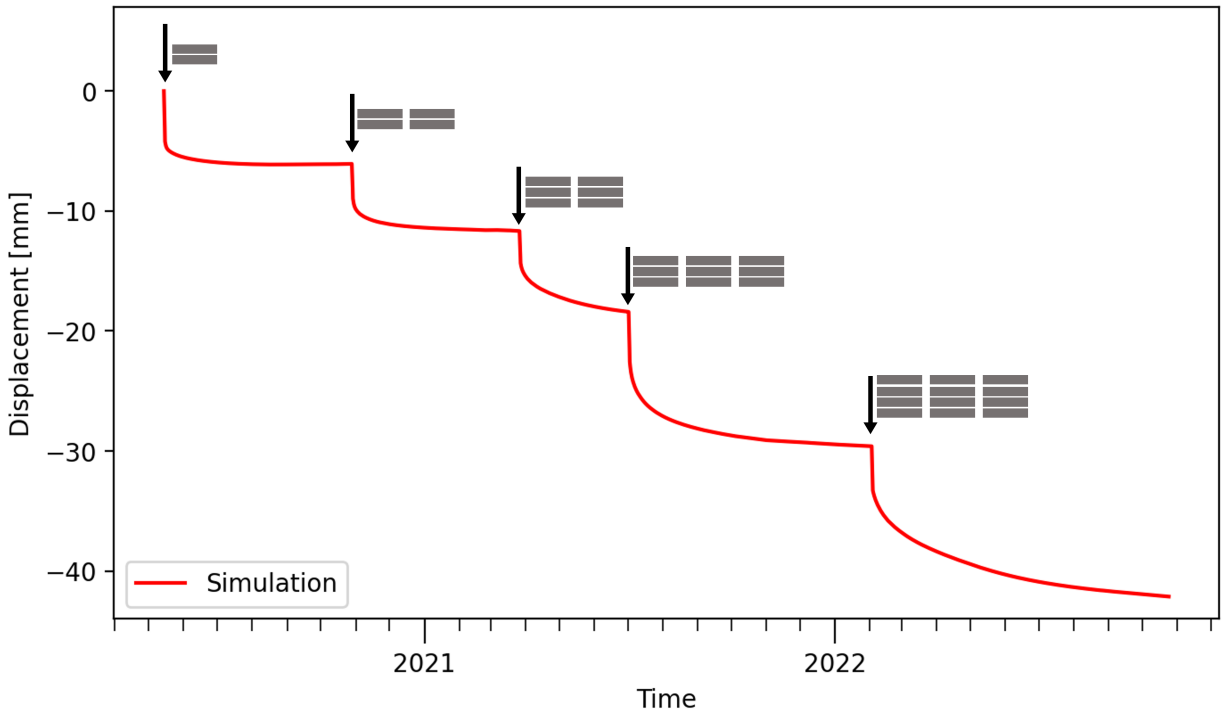

Figure 6.3: Model simulation of the settlements at the pile foot, showing each loading with the total number of added concrete slabs.

One reason for this is that the immediate settlement after loading is determined by the added incremental loading, while the creep settlement is determined by the total applied load. Whilst the incremental loading is relatively similar for each loading step, as seen in Table 5.5, the total load increases significantly more with each

step. Another reason for the disproportionately big immediate settlement after the first loading is that compression and hardening of the soil will make the immediate settlement smaller for each equally incremental load. Whilst the clay layer has been preconsolidated to some degree by overlying sediments, the thin sand layer placed below each footing might not have been preconsolidated, leading to bigger immediate settlements at the primary loading.

6.2 Simulated Temperature

The comparison of temperature at the pile tip for the simulation and logged data is shown in Figure 6.4. The simulated temperature is generally 0.5 to 1 °C warmer than the measured temperature, which is a big deviation for a ground temperature that has an annual variation of 1.5 °C.

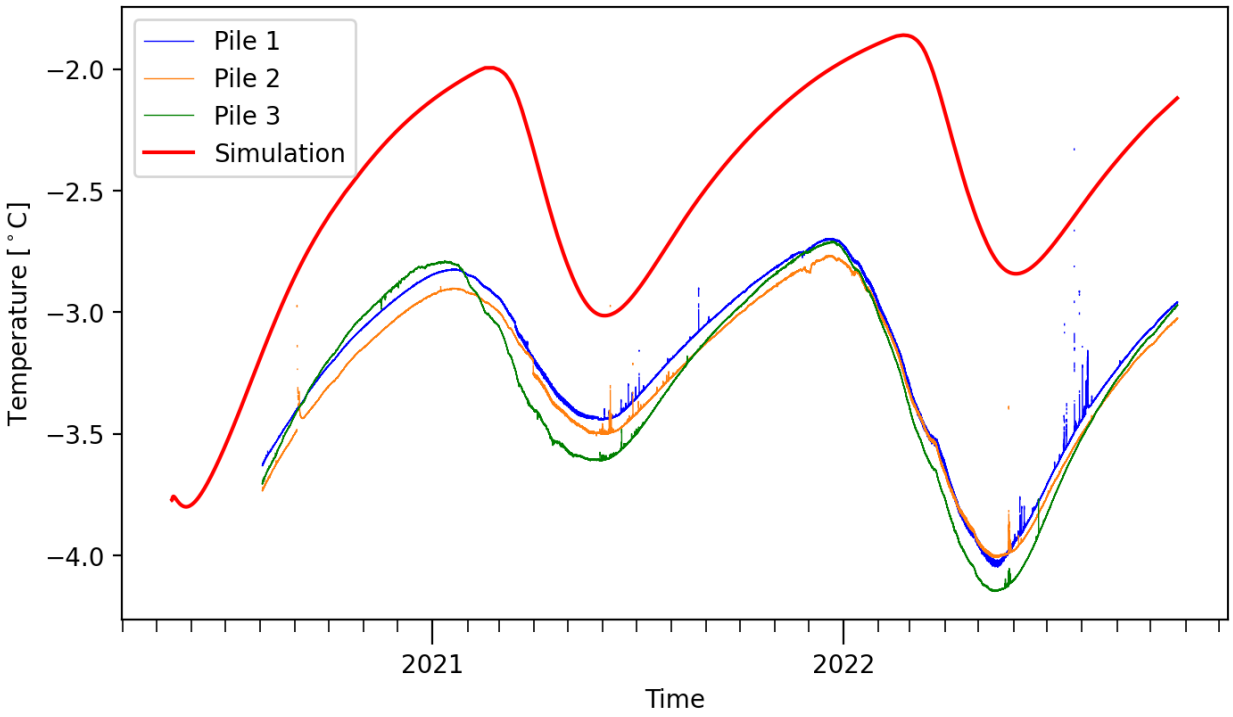

Figure 6.4: Model simulation of the temperature at the pile foot along with data measurements from thermistors at the pile foot.

During the simulations, it was discovered that PLAXIS V21.1 and the implemented code for the elasto-viscoplastic model used to model the marine clay layer are not completely compatible. Because of this, the latent heat of phase change is not accounted for. As described in Section 2.3.4 energy will be released when water freezes to ice, and absorbed when the ice melts. This is an important phenomenon to account for in order to predict the soil's ground thermal regime accurately and can explain some of the deviations in the simulated ground temperature. This is further elaborated in Chapter 7.

Figure 6.5 presents the simulated temperature at the pile tip, along with the temperature boundary condition at the ground surface. The figure shows how the ground temperature is attenuated with depth. At the pile tip (4

m depth), the fluctuations are 1.5 °C, whilst at the ground surface they are over 20 °C throughout the year. This is due to the thermal diffusivity of the soil, as explained in Section 2.1. The figure also shows the delay in maximum and minimum temperature from the surface and further down in the sediments. Whilst the simulated surface temperature has its maximum in August, the temperature at the pile tip has its maximum around February. This corresponds well with the theory in Section 2.1.

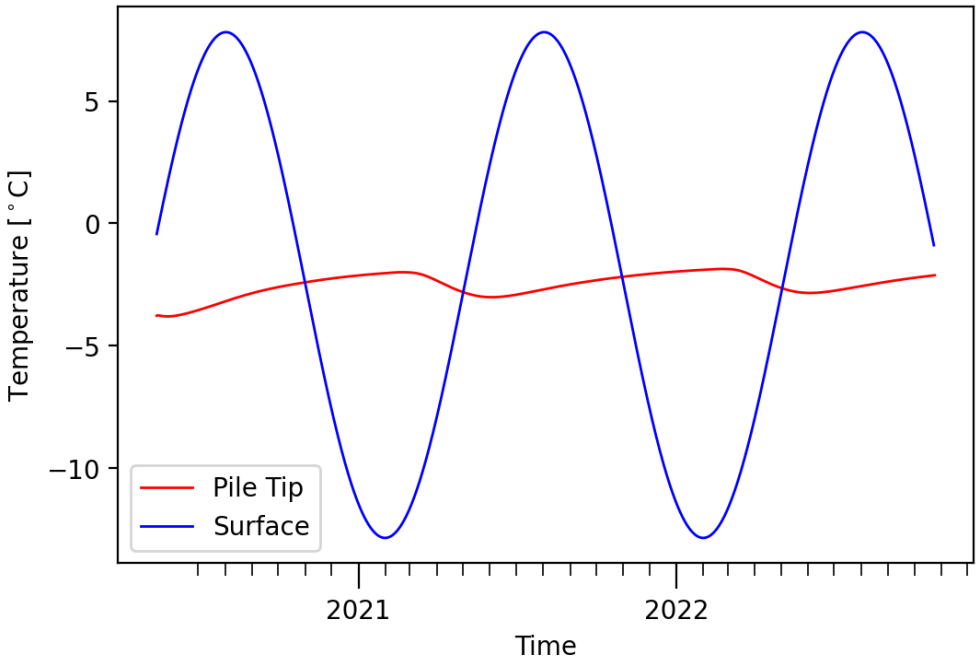

Figure 6.5: Temperature boundary condition at the ground surface along with simulated temperature the pile tip.

A demonstration of how the temperature varies with depth throughout the seasons is given in Figure 6.6. A big resemblance between the simulated temperature in this figure and the illustration in Figure 2.1 can be seen. Whilst the temperature variations are big at the surface, they quickly decrease with depth. From a depth of about 10 meters, the variations are negligible and go towards the zero annual amplitude (ZAA). However, the temperature decreases until a depth of approximately 25 meters. From this point, it appears that the temperature begins to increase. It is expected that the temperature will continue to increase approximately linearly with depth due to the heat flow from the earth's interior to the surface.

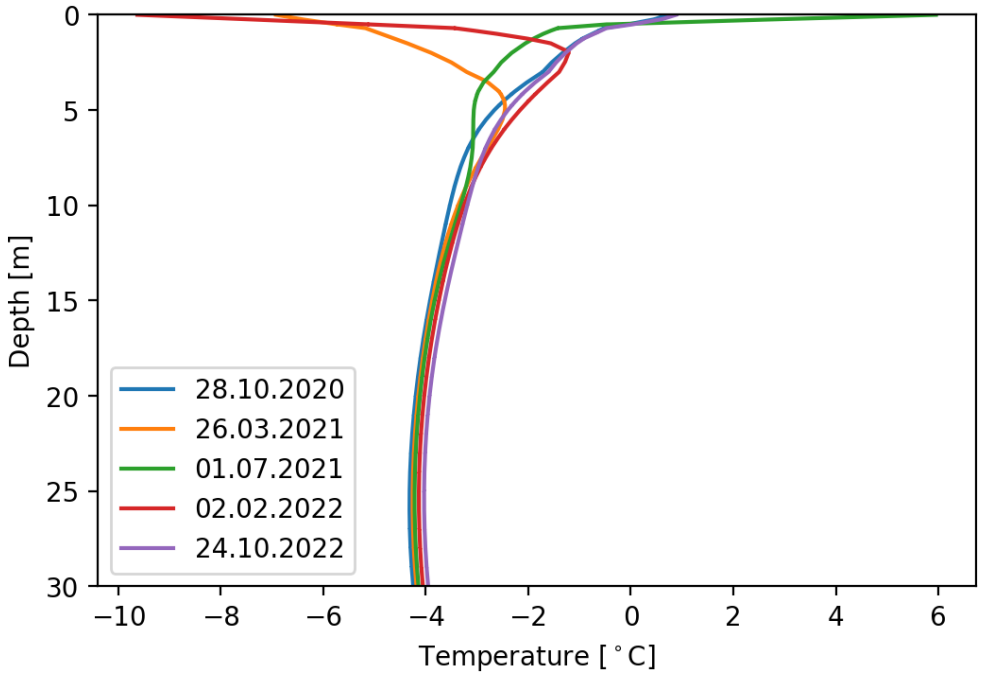

Figure 6.6: Simulated temperature with depth at the end of each creep phase.

Chapter 7

Discussion

In this chapter a discussion of the obtained results will be presented. This includes the consequences of different assumptions and simplification used in the numerical model on the simulated results, and also possible sources of error explaining the deviation between the experimental data and the numerical simulations.

7.1 Assumptions Regarding the Surface Temperature

For the temperature boundary condition at the ground surface, a constant sinusoidal function has been used, as seen in Figure 4.5. The function is based on the measured surface temperature from thermistor E5. However, even though the sinusoidal function is constant, a slight variation in ground temperature from year to year can be seen from the simulation in Figure 6.4. For example, 2022 gives a slightly warmer maximum and minimum temperature than 2021. This can be explained by the initial temperature condition in the soil provided by thermistor E5 as described in Section 5.4. As the initial temperature condition is colder than the calculated temperature based on the surface conditions in the model, the average annual ground temperature at the pile tip will slightly increase each year until the effect of the initial state can be neglected. For this experiment, it was not considered significant to include the interannual variations in surface temperature, as the time period is just about two years. For a long-term simulation over several years or decades, a surface boundary condition that will vary from year to year should be used to capture the temperature variations due to both local conditions and global warming.

Instead of using the sinusoidal function as the surface boundary condition, it would have been possible to use the exact surface temperature from thermistor E5. The main reason for not doing this was that the temperature data at thermistor E5 has several periods with missing data, and it was therefore decided to use a smoother function. From Figure 4.5, it is clear that the measured temperature has a greater annual maximum and minimum than the sinusoidal function. However, it is not expected that this will significantly impact the simulated temperature further down in the ground, as the average seasonal temperature should be approximately the same. Since the surface temperature condition is based on the temperature at the nearby thermistor E5, there might be a deviation from the actual surface temperature at the pile loading test site. However, it is expected that the surface temperature

variation over the surface area is small and that any possible deviation is therefore insignificant.

7.2 Simplifications in the Numerical Model

The numerical model will be a simplification of reality, as mentioned in Section 1.3. The soil polygon is divided into three perfectly homogeneous soil layers, while each layer in reality will never be completely homogeneous. Furthermore, no soil samples have been tested from the two sand layers overlying the marine clay. As a consequence, the mechanical properties of these layers have a big uncertainty and are mostly based upon the information given in Gilbert et al. [2019]. For simplicity and lack of information, the sand layers are assumed to be linear elastic. However, it is not expected that this has a big impact on the results, as the pile footings are installed one meter down in the marine clay layer and the results are therefore mainly dependent on the properties of this layer.

Moreover, the soil samples used to decide the parameters for the marine clay layer are all taken from the same borehole, as indicated in Figure 4.3. As mentioned earlier in Section 4.3, the soil will never be completely homogeneous and local variations in soil properties are expected. To account for local variations soil samples should therefore preferably be taken from several boreholes. This can decrease the uncertainty regarding the determination of parameters for the soil properties.

7.3 Ground Temperature Deviation

There is a deviation between the simulated settlement and the logged settlements at the pile tip of about 0.5 to 1 °C, as mentioned in Chapter 6. In Chapter 6 it is also stated that the PLAXIS software V21.1 does not account for the latent heat of phase change when the elasto-viscoplastic model is used, which can explain parts of the ground temperature deviation at the pile tip. Energy will be released when liquid water freezes to ice, and absorbed when ice melts as explained in Section 2.3.4. Neglecting the phase change energy in the temperature calculations leads to an overestimate of the temperature when pore water melts and an underestimate of the temperature when pore water freezes to ice. In addition, the phase change will happen faster when the latent heat is neglected, leading to a quicker change of temperature in the soil. In Figure 6.4 one can see that the offset between the simulated and measured temperature varies from around 0.5 to 1 °C, being largest at the temperature peaks and lowest at the temperature troughs, making the slope of the simulated temperature steeper than that of the experimental data. This is a consequence of the neglected latent heat, as the energy is overestimated when pore water melts during the warmer periods and underestimated when pore water freezes during the colder periods.

However, the absence of phase change energy cannot explain the entire ground temperature offset. If the latent heat was included, there would still be a temperature deviation, but the offset is expected to be smaller and more constant. A source of the remaining error may come from the initial temperature condition. The initial condition was taken from thermistor E5, situated nearby the footing test site, as seen in Figure 4.1b. As stated earlier in Section 4.3, the temperature sensors started logging data at the beginning of August 2020, thus one does not have access

to the accurate temperature distribution at the beginning of the pile loading test. According to Lyu et al. [2021b] the construction of the test site during the winter 2020 gave an additional cooling of the soil from -3.1±0.3 °C to down below -5 °C. Therefore, there might be an offset between the simulation and the experimental data already introduced by the initial condition. This can also be seen by looking at Figure 6.4, where the simulated temperature at the beginning of the time period in May 2020 is almost the same as the measured temperature from August 2020. It is expected that the ground temperature at the pile tip is lower in May than in August due to annual variations, as can be seen by the measured temperature for 2021 and 2022.

7.4 Temperature-dependent Creep Rate

The experimental data shows an immediate settlement after loading but also a change in creep rate as the temperature increases towards -3 °C, which is also mentioned in Chapter 6. The simulations do not show this change in creep rate and are heavily dominated by immediate settlements. This deviation in creep behaviour must be seen alongside the deviations in simulated temperature at the pile tip. However, the lack of temperature dependency in the simulated settlements may stem from N, often referred to as the creep ratio. The creep rate is determined by several equations given in Section 3.3, but is heavily dependent on Equation 3.22, describing the viscoplastic strain increment due to variation of the solid phase stress. The creep ratio, N, says something about how strain rate sensitive the material is. It can be seen as a comparison of plastic and viscoplastic behaviour. As mentioned in Section 2.3.1 will frozen soils in general be more rate sensitive than the corresponding unfrozen soil. A big value of N means that the material is less rate sensitive, whilst a small value of N leads to a more rate sensitive material. The viscoplastic strain will happens faster for a big value of N, making it less time-dependent, closer to that expected from a completely plastic behaviour. This can be seen as a less creepy behaviour, by defining creepy behaviour like settlements which happens over a longer time period. In the model formulation the creep ratio is given by Equation 3.25, replicated below

$$N = N_0 + b_1 \times S(T) - b_2 \times s_i(T). \tag{3.25}$$

As seen by Equation 3.25, N will vary with ice content s_i and suction S. In the model formulation, this variation is expressed as a linear combination of both the ice content and the suction. As both the ice content and the cryogenic suction are dependent on temperature, N can therefore be expressed as a function of temperature, as seen in Figure 7.1. The figure shows an almost linear increase in N with decreasing temperatures from about -8 °C and lower, leading to a behaviour closer to that of a plastic material. Such a steep increase in N is highly unrealistic, and the linear construction of N given in Equation 3.25 is a simplification of reality, and not that applicable. The purpose of implementing this function in the model formula is to show that N will vary with suction and ice content, and cannot be treated as a constant parameter as it normally does in unfrozen soil. However, ideally, the dependency of ice content and suction on N should be investigated more closely and a more accurate formulation should be used. The simulated temperatures at the pile tip range from -3.8 to -1.8 °C as seen in Figure 6.4, giving a range in N from

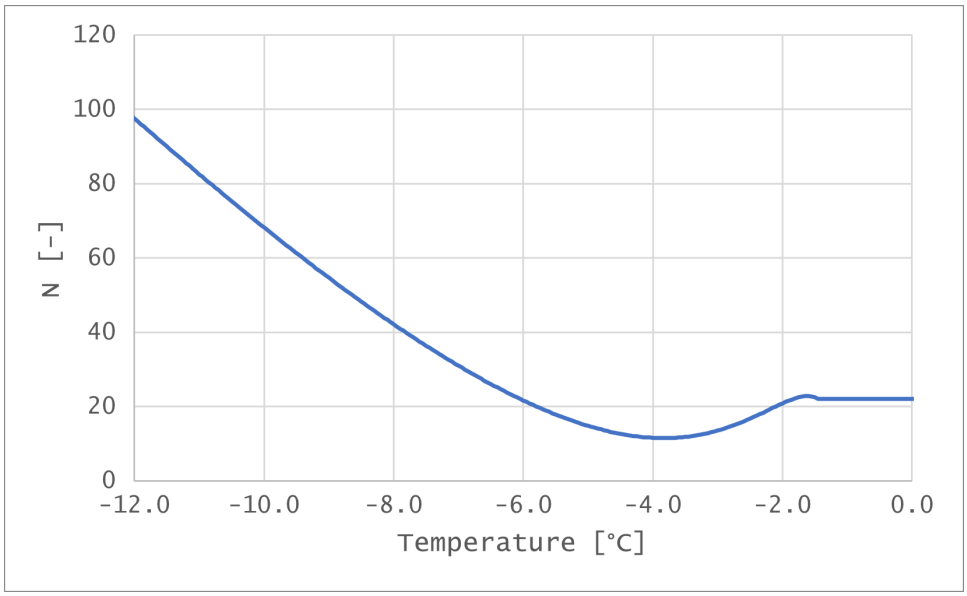

Figure 7.1: The strain rate coefficient, N, as a function of temperature

11.5 to 22.2, shown in Figure 7.1. This is expected to be a big enough change in the strain rate coefficient to give a noteworthy change in creep rate. However, the simulated results show that this is not the case. It may be that a stronger temperature dependency could have been achieved with lower values of N, making the material more rate sensitive and therefore showing a more creepy behaviour The numerical constants, N_0, b_1 and b_2, which determine N have been decided based on numerical calibration against laboratory triaxial creep tests carried out on samples taken from the pile loading test site, as described in Section 5.2. It would not be realistic to change these values to get better results for the simulation, as they would not fit with the calibration of the creep test results. Therefore, according to the linear function assigned for N in the model, and the triaxial creep test results, it is hard to achieve a better accuracy than the one which is presented in this thesis.

7.5 Knowledge of the Numerical Model

In Section 1.3, the limitations, it is mentioned how knowledge about the software is essential to get simulations with an acceptable accuracy. Even though the model parameters are determined with a high level of accuracy, other problems can arise, such as the compatibility issues described above where the phase change energy is neglected, leading to lower accuracy and increased uncertainty. A good understanding of PLAXIS and the implemented model is therefore necessary to detect such issues. Compatibility issues make it harder to determine whether deviations in the simulations are due to the compatibility issues, the accuracy of the model or the knowledge and expertise of the user.

Previously, similar studies have been done on the elasto-viscoplastic model used in this thesis. Ghoreishian and Grimstad [2017] used the same model to simulate a long-term loading experiment, not too different from the pile loading test used in this thesis. The results showed a good correlation between the simulated and measured

settlements. Moreover, the simulations showed a temperature-dependent creep rate, which this thesis has not achieved. The simulated creep rate changed very step-wise, similar to several immediate settlements after loading. It is uncertain if the model can simulate a more subtle change in creep rate. Ghoreishian and Grimstad [2017] also used the PLAXIS software, but a previous version, most likely PLAXIS V16. The code of the elasto-viscoplastic model was made in 2015/2016 and is expected to have been fully compatible with the 2016 version of PLAXIS. This shows that the model is able to simulate temperature-dependent creep behaviour when not obstructed by compatibility issues. A decisive factor in making the model work has been the help and guidance of Seyed Ali Ghoreishian Amiri, who was primarily responsible for developing the elasto-viscoplastic model. Without his insight, it would have been challenging to detect the compatibility issues and understand how they affect the achieved results.

7.6 Importance of Numerical Modelling of Frozen Soils

The results in Chapter 6 show that the model can simulate the settlements with an acceptable accuracy at the end of the time period, even though there is a deviation in creep behaviour throughout the simulation. The error estimate might grow if the problem is simulated for an extended time period. Achieving an acceptable level of accuracy requires a lot of effort when it comes to the determination of parameters. It must be carried out index and properties tests on soil samples from the relevant area and thereafter numerical calibration to achieve sufficient accuracy levels. Smaller projects which do not have the possibility to carry out field investigations must, to a greater extent, lean on empirical methods and principles for determining the bearing capacity and the settlements. The annual temperature in polar regions has been increasing for the last few decades and is expected to keep rising towards the 22nd century [AMAP, 2017]. Traditionally, the ground conditions in permafrost have been stable and reliable, making empirical methods a good approach. However, as the ground conditions rapidly change, this will no longer be the case. Therefore, field investigations and model simulations will play a more significant part in determining the bearing capacity and expected settlements when designing foundations in permafrost in the future. When designing foundations, it is essential to use a sufficient safety factor to account for the uncertainty in the calculations. A safety factor must also account for the uncertainty of the ground conditions and the expected degradation of permafrost in the future. A considerable uncertainty in the simulations will require a big safety margin. Consequently, executing more field investigations, doing a thorough job with the model set-up- and parameter determination can affect the necessary safety factor and influence the project's total cost.

Chapter 8

Conclusion

8.1 Summary and Conclusion

Global warming will inevitably have a big impact on the temperature in Arctic regions, as it is estimated that the temperature in the Arctic will rise by 4-5 °C from the end of the 20th century to 2050 [AMAP, 2017]. This will lead to the warming and degradation of permafrost, giving geotechnical challenges in areas where one could earlier assume a stable, reliable permafrost layer. The mechanical properties of frozen soils are generally much more temperature dependent than those of unfrozen soils. Warm permafrost, with a ground temperature close to the melting point, is particularly sensitive to temperature change, and a small temperature rise can have a significant impact on the soil conditions. A temperature rise will also lead to a thickening of the active layer, which amongst other things can give increased problems with spring thawing. A larger extent of warm permafrost will lead to a bigger uncertainty in the soil conditions, increasing the need for accurate frozen soil models. As the soil conditions are rapidly changing, previous empirical methods will be less relevant and it is expected that the use of numerical models will increase.

The elasto-viscoplastic model described in Chapter 3 is used to simulate the ground thermal regime and the footing settlements in the marine clay. The strength of the materials is well described in the numerical model, as the simulated settlements given in Chapter 6 coincide well with the experimental data, especially for Pile 1 and 3. Therefore one can conclude that the strength parameters in the model have sufficient accuracy. However, as discussed in Chapter 7, there is a deviation between the experimental and simulated settlements in creep behaviour throughout the simulated time period. The experimental data shows an immediate settlement after loading, but also a change in creep rate as the ground temperature increases towards -3 °C. The simulations do not show this change in creep behaviour and are heavily dominated by immediate settlements. This deviation can be seen clearly in Figure 6.2. The main reason for this deviation comes from the formulation of the creep ratio N, which is formulated as a linear function of the cryogenic suction and the ice content. Such a linear dependency on the ice content and suction of N is not very realistic. Ideally, the relationship between the parameters should be investigated closer

to achieve a more accurate formulation. The numerical constants which determine N have been decided based on the numerical calibration of triaxial creep tests taken of samples from the test site. Changing these values to adjust for the observed deviation would not be appropriate, as the parameters should be decided based on experimental test results from the site.

Furthermore, there is a deviation between the simulated and measured ground temperatures at the pile footing of approximately 0.5 to 1 °C. This deviation is a result of neglecting latent heat from the phase change between ice and water. Due to compatibility issues between the PLAXIS V21.1 software and the elasto-viscoplastic model code, the latent heat of phase change will not be accounted for when calculating the ground thermal regime, leading to a discrepancy between the measured and simulated temperature. Another error source for the temperature offset is the given initial temperature condition as there is no available temperature data from the test site for the three first months of the test. Therefore the initial condition is taken from a nearby thermistor, and it is hard to determine if this coincides well with the genuine thermal regime at the beginning of the footing test.

The frozen soil model used in this thesis can be a good tool when designing foundations in permafrost areas. Even though some discrepancies between the experimental and simulated results are observed, the total settlements at the end of the simulated time period are of the same magnitude as the experimental data. Therefore, the model can give an estimate of the expected foundation settlements. In addition, safety factors in accordance with national regulations must be used in the design of foundations to account for uncertainties. It is important to keep in mind that the numerical simulations are an estimate of the future, and cannot be treated as fact. In geotechniques, there are a lot of uncertainties, not only when it comes to the numerical model, but also in the properties of the soil. As mentioned earlier, the soil will never be completely homogeneous and the determined soil properties will be a simplification of reality.

8.2 Recommendations for Future Work

For further work within the topic, the following actions are recommended:

- In the model formulation the temperature dependency of the creep rate is amongst others dependent of the creep ratio, N. The coefficient is formulated as a linear function of the ice content and cryogenic suction, which is a simplified approximation of the relationship. To improve the creep rate accuracy, this relationship should be examined further to define a more precise formulation for N.

- To obtain a precise prediction of the ground thermal regime it is essential to account for the latent phase change energy. Due to compatibility issues between the PLAXIS V21.1 software and the frozen soil model code, the latent heat of phase change is neglected in the temperature calculations. For further development of the model, this compatibility issue should be examined and solved.

- Advanced numerical soil models, such as the elasto-viscoplastic soil model used in this thesis, require an extensive lab program to determine the model parameters. To reduce the workload of parameter determina-

tion the use of reference parameter sets from previous parametric studies on frozen soils can be utilised. For several other advanced numerical soil models, this already exists. By collecting results from several lab tests on a variety of soils a register of the relation between different parameters can be established. For instance, by collecting data on the grain size distribution, salt content and freezing temperature of a variety of frozen soils, an estimate of the freezing temperature can be found from the salt content and grain size distribution without needing to do spesific laboratory tests to find this.

Bibliography

E. E. Alonso, A. Gens, and A. Josa. A constitutive model for partially saturated soils. *Géotechnique*, 40(3):405–430, 1990.

AMAP. Snow, water, ice and permafrost in the arctic (swipa). Technical report, Arctic Monitoring and Assessment Programme (AMAP), Oslo, Norway, 2017.

S. A. G. Amiri, G. Grimstad, and M. Kadivar. An elastic-viscoplastic model for saturated frozen soils. *European Journal of Environmental and Civil Engineering*, 26(7):2537–2553, 2016a. doi: 10.1080/19648189.2016.1271361. URL https://doi.org/10.1080/19648189.2016.1271361.

S. A. G. Amiri, G. Grimstad, M. Kadivar, and S. Nordal. Constitutive model for rate-independent behavior of saturated frozen soils. *Canadian Geotechnical Journal*, 53(10):1646–1657, 2016b. doi: 10.1139/cgj-2015-0467. URL https://doi.org/10.1139/cgj-2015-0467.

O. B. Andersland and D. Anderson. *Geotechnical Engineering for Cold Regions*. McGraw-Hill, 1978. ISBN 9780070016156. URL https://books.google.no/books?id=0259QgAACAAJ.

O. B. Andersland and B. Ladanyi. *Frozen Ground Engineering*. John Wiley & Sons, Inc., Hoboken, New Jersey, 2004.

L. U. Arenson and S. M. Springman. Mathematical descriptions for the behaviour of ice-rich frozen soils at temperatures close to 0 °c. *Canadian Geotechnical Journal*, 42(2):431–442, 2005. doi: 10.1139/t04-109. URL https://doi.org/10.1139/t04-109.

L. U. Arenson, M. M. Johansen, and S. M. Springman. Effects of volumetric ice content and strain rate on shear strength under triaxial conditions for frozen soil samples. *Permafrost and Periglacial Processes*, 15(3):261–271, 2004.

T. Baker. Strain rate effect on the compressive strength of frozen sand. *Engineering Geology*, 13(1):223–231, 1979. ISSN 0013-7952. doi: https://doi.org/10.1016/0013-7952(79)90034-6. URL https://www.sciencedirect.com/science/article/pii/0013795279900346. Ground Freezing.

Bentley. *PLAXIS 2D CE V22.01: 2 - Reference Manual*. Bentley, 2021.

R. J. E. Brown and W. O. Kupsch. Permafrost terminology. Technical report, National Research Council of Canada. Associate Committee on Geotechnical Research, 12 1974. URL https://doi.org/10.4224/20378592.

E. Chamberlain, C. Groves, and R. Perham. The mechanical behaviour of frozen earth materials under high pressure triaxial test conditions. *Géotechnique*, 22(3):469–483, 1972. doi: 10.1680/geot.1972.22.3.469. URL https://doi.org/10.1680/geot.1972.22.3.469.

Z. Chen, X. Guo, L. Shao, S. Li, and L. Gao. Sensitivity analysis of the frozen soil nonlinear latent heat and its precise transformation method. *Geophysical Journal International*, 228(1):240–249, 08 2021. ISSN 0956-540X. doi: 10.1093/gji/ggab319. URL https://doi.org/10.1093/gji/ggab319.

B. Etzelmüller, T. V. Schuler, K. Isaksen, H. H. Christiansen, H. Farbrot, and R. Benestad. Modeling the temperature evolution of svalbard permafrost during the 20th and 21st century. *The Cryosphere*, 5(1):67–79, 2011. doi: 10.5194/tc-5-67-2011. URL https://tc.copernicus.org/articles/5/67/2011/.

E. J. Førland, R. Benestad, I. Hanssen-Bauer, J. E. Haugen, and T. E. Skaugen. Temperature and precipitation development at svalbard 1900–2100. *Advances in Meteorology*, 2011, 2011.

H. M. French. *The periglacial environment*. John Wiley & Sons, 2017.

R. W. Gerdel. Characteristics of the cold regions. Technical report, Cold Regions Research and Engineering Laboratory (U.S.), 1969. URL http://hdl.handle.net/11681/2650.

A. Ghoreishian and G. Grimstad. Constitutive model for long-term behavior of saturated frozen soil. In *Proc of the 6th Biot Conf. on Poromechanics*, pages 1005–12, 2017.

G. Gilbert, A. Instanes, A. Sinitsyn, and A. Aalberg. Characterization of two sites for geotechnical testing in permafrost: Longyearbyen, svalbard. *AIMS Geosciences*, 5(4):868–885, 2019. ISSN 2471-2132. doi: 10.3934/geosci.2019.4.868. URL https://www.aimspress.com/article/doi/10.3934/geosci.2019.4.868.

U. H. Haug Bratlie. An experimental study of thermal properties of permafrost soils. Master's thesis, Norwegian University of Science and Technology, Trondheim, Norway, 7 2018.

T. F. Hennum. Fundamenteringsmetoder i områder med permafrost og konsekvenser av global oppvarming, 2022. Project thesis.

J. Hjort, O. Karjalainen, J. Aalto, S. Westermann, V. E. Romanovsky, F. E. Nelson, B. Etzelmüller, and M. Luoto. Degrading permafrost puts arctic infrastructure at risk by mid-century. *Nature communications*, 9(1):1–9, 2018.

H.-C. Huang. Experimental study on creep of frozen marine fine-grained soil in longyearbyen, svalbard. Master's thesis, Norwegian University of Science and Technology, Trondheim, Norway, 11 2020.

A. Instanes. Incorporating climate warming scenarios in coastal permafrost engineering design – case studies from svalbard and northwest russia. *Cold Regions Science and Technology*, 131:76–87, 2016. ISSN 0165-232X.

doi: https://doi.org/10.1016/j.coldregions.2016.09.004. URL https://www.sciencedirect.com/science/article/pii/S0165232X1630180X.

N. P. Institute. Svalbardkartet, 2022a. URL https://geokart.npolar.no/Html5Viewer/index.html?viewer=Svalbardkartet.

N. P. Institute. Toposvalbard, 2022b. URL https://toposvalbard.npolar.no/.

Y. Lai, S. Li, J. Qi, Z. Gao, and X. Chang. Strength distributions of warm frozen clay and its stochastic damage constitutive model. *Cold Regions Science and Technology*, 53(2):200–215, 2008. ISSN 0165-232X. doi: https://doi.org/10.1016/j.coldregions.2007.11.001. URL https://www.sciencedirect.com/science/article/pii/S0165232X07001929.

N. Li, F. Chen, B. Xu, and G. Swoboda. Theoretical modeling framework for an unsaturated freezing soil. *Cold Regions Science and Technology*, 54(1):19–35, 2008. ISSN 0165-232X. doi: https://doi.org/10.1016/j.coldregions.2007.12.001. URL https://www.sciencedirect.com/science/article/pii/S0165232X07001978.

C. Lyu. *Mechanical behavior of frozen saline clay: laboratory, field and numerical investigation.* PhD thesis, NTNU, Trondheim, Norway, 10 2021.

C. Lyu, G. Grimstad, K. Rieksts, S. A. G. Amiri, A. Aalberg, and T. Ingeman-Nielsen. Consequences of global warming on marine saline permafrost - case of longyearbyen. *Engineering Geology*, 2021a.

C. Lyu, A. Shestov, G. Eiksund, S. Nordal, K. Høyland, G. Grimstad, and A. Aalberg. Field footing test for foundation settlement estimate of marine saline permafrost in longyearbyen, svalbard. In *Proceedings of the 20th International Conference on Soil Mechanics and Geotechnical Engineering. Edited by ICSMGE, Sydney*, 2021b.

C. Lyu, F. Zhu, G. Grimstad, K. V. Høyland, and S. A. G. Amiri. Consequences of global warming on infrastructure settlement in permafrost - case of longyearbyen. 2021c.

D. Nicolsky, V. Romanovsky, G. Tipenko, and D. Walker. Modeling biogeophysical interactions in nonsorted circles in the low arctic. *Journal of Geophysical Research: Biogeosciences*, 113(G3), 2008.

S. Nishimura, A. Gens, S. Olivella, and R. J. Jardine. Thm-coupled finite element analysis of frozen soil: formulation and application. *Géotechnique*, 59(3):159–171, 2009. doi: 10.1680/geot.2009.59.3.159. URL https://doi.org/10.1680/geot.2009.59.3.159.

J. F. D. Nixon. Discrete ice lens theory for frost heave in soils. *Canadian Geotechnical Journal*, 28(6):843–859, 1991. doi: 10.1139/t91-102. URL https://doi.org/10.1139/t91-102.

NSIDC. Cryosphere glossary, frozen ground or permafrost, 2022. URL https://nsidc.org/cryosphere/glossary-terms/frozen-ground-or-permafrost.

Nunataryuk Project. Nunataryuk, 2021. URL https://nunataryuk.org.

P. Perzyna. Fundamental problems in viscoplasticity. *Advances in applied mechanics*, 9:243–377, 1966.

D. W. Riseborough and M. W. Smith. Modelling permafrost response to climate change and climate variability. In *Proceedings, Fourth International Symposium on Thermal Engineering & Science for Cold Regions*, pages 179–187, Hanover, New Hampshire, 1993. US Army Cold Regions Research and Engineering Laboratory, Special Report.

H. R. Thomas, P. Cleall, Y.-C. Li, C. Harris, and M. Kern-Luetschg. Modelling of cryogenic processes in permafrost and seasonally frozen soils. *Géotechnique*, 59(3):173–184, 2009. doi: 10.1680/geot.2009.59.3.173. URL https://doi.org/10.1680/geot.2009.59.3.173.

S. Vyalov and G. Porkhaev. Handbook for the design of bases and foundations of buildings and other structures on permafrost. Technical report, National Research Council of Canada. Division of Building Research. Oversettelse TT 1865, 1976. URL https://nrc-publications.canada.ca/eng/view/object/?id=19cf94f2-9d2c-4fa1-9c30-a91d027d23d5.

Q. Wang, J. Fang, X. Zhao, and K. Hu. The influence of pavement type on the thermal stability of block-stone embankments in the warm permafrost region. *Transportation Geotechnics*, 23:100334, 2020. ISSN 2214-3912. doi: https://doi.org/10.1016/j.trgeo.2020.100334. URL https://www.sciencedirect.com/science/article/pii/S2214391219301564.

M. Wei, C. Guodong, and W. Qingbai. Construction on permafrost foundations: Lessons learned from the qinghai–tibet railroad. *Cold Regions Science and Technology*, 59(1):3–11, 2009. ISSN 0165-232X. doi: https://doi.org/10.1016/j.coldregions.2009.07.007. URL https://www.sciencedirect.com/science/article/pii/S0165232X09001335.

J. S. Wettlaufer and M. G. Worster. Premelting dynamics. *Annual Review of Fluid Mechanics*, 38(1):427–452, 2006.

P. J. Williams and M. Wallis. Permafrost and climate change: Geotechnical implications [and discussion]. *Philosophical Transactions: Physical Sciences and Engineering*, 352(1699):347–358, 1995. ISSN 09628428. URL http://www.jstor.org/stable/54455.

X. Yao, J. Qi, J. Zhang, and F. Yu. A one-dimensional creep model for frozen soils taking temperature as an independent variable. *Soils and Foundations*, 58(3):627–640, 2018. ISSN 0038-0806. doi: https://doi.org/10.1016/j.sandf.2018.03.001. URL https://www.sciencedirect.com/science/article/pii/S0038080618300374.

Y. Zhang and R. L. Michalowski. Thermal-hydro-mechanical analysis of frost heave and thaw settlement. *Journal of Geotechnical and Geoenvironmental Engineering*, 141(7):04015027, 2015. doi: 10.1061/(ASCE)GT.1943-5606.0001305. URL https://ascelibrary.org/doi/abs/10.1061/%28ASCE%29GT.1943-5606.0001305.

M.-M. Zhou. *Computational simulation of soil freezing: multiphase modeling and strength upscaling*. PhD thesis, Ruhr-Universität Bochum, Fakultät für Bau-und Umwelt-Ingenieurwissenschaften, 2014.

Z. Zhu, J. Ning, and W. Ma. A constitutive model of frozen soil with damage and numerical simulation for the coupled problem. *Science China Physics, Mechanics and Astronomy*, 53(4):699–711, 2010.

PLAXIS Model; Calculations and Result

In this appendix, additional information regarding the calculation and results from PLAXIS are presented. This includes the phase settings in PLAXIS and figures showing the element mesh, vertical displacement and temperature distribution of the soil polygon.

ID	Calculation t...	Loading type...	Pore pressur...	Time interval	Estimated en...	Ignore undr....	Reset displa...	Updated me...	Max steps (D)	First step	Last step
Initial phase [InitialPhase]	**K0**			**0,000 s**	**0,000 s**	☑	☐	☐	**1000**	**0**	**0**
Equilibrium [Phase_1]	Ful			100,0E6 s	100,0E6 s	☐	☑	☐	1000	1	14
Excavation [Phase_2]	Ful			86,40E3 s	100,1E6 s	☐	☐	☐	1000	15	28
Waiting [Phase_13]	Ful			527,0E3 s	100,6E6 s	☐	☐	☐	1000	29	42
Loading 1 [Phase_3]	Ful			86,40E3 s	86,40E3 s	☐	☑	☐	1000	43	56
Creep 1 [Phase_4]	Ful			14,34E6 s	14,43E6 s	☐	☐	☐	1000	683	766
Loading 2 [Phase_5]	Ful			86,40E3 s	14,52E6 s	☐	☐	☐	1000	57	70
Creep 2 [Phase_6]	Ful			12,79E6 s	27,30E6 s	☐	☐	☐	1000	71	165
Loading 3 [Phase_7]	Ful			86,40E3 s	27,39E6 s	☐	☐	☐	1000	166	179
Creep 3 [Phase_8]	Ful			8,294E6 s	35,68E6 s	☐	☐	☐	1000	767	933
Loading 4 [Phase_9]	Ful			86,40E3 s	35,77E6 s	☐	☐	☐	1000	180	193
Creep 4 [Phase_10]	Ful			18,58E6 s	54,35E6 s	☐	☐	☐	1000	194	282
Loading 5 [Phase_11]	Ful			86,40E3 s	54,43E6 s	☐	☐	☐	1000	283	296
Creep 5 [Phase_12]	Ful			22,72E6 s	77,16E6 s	☐	☐	☐	1000	297	480

Figure 1: Phase settings used in PLAXIS calculation.

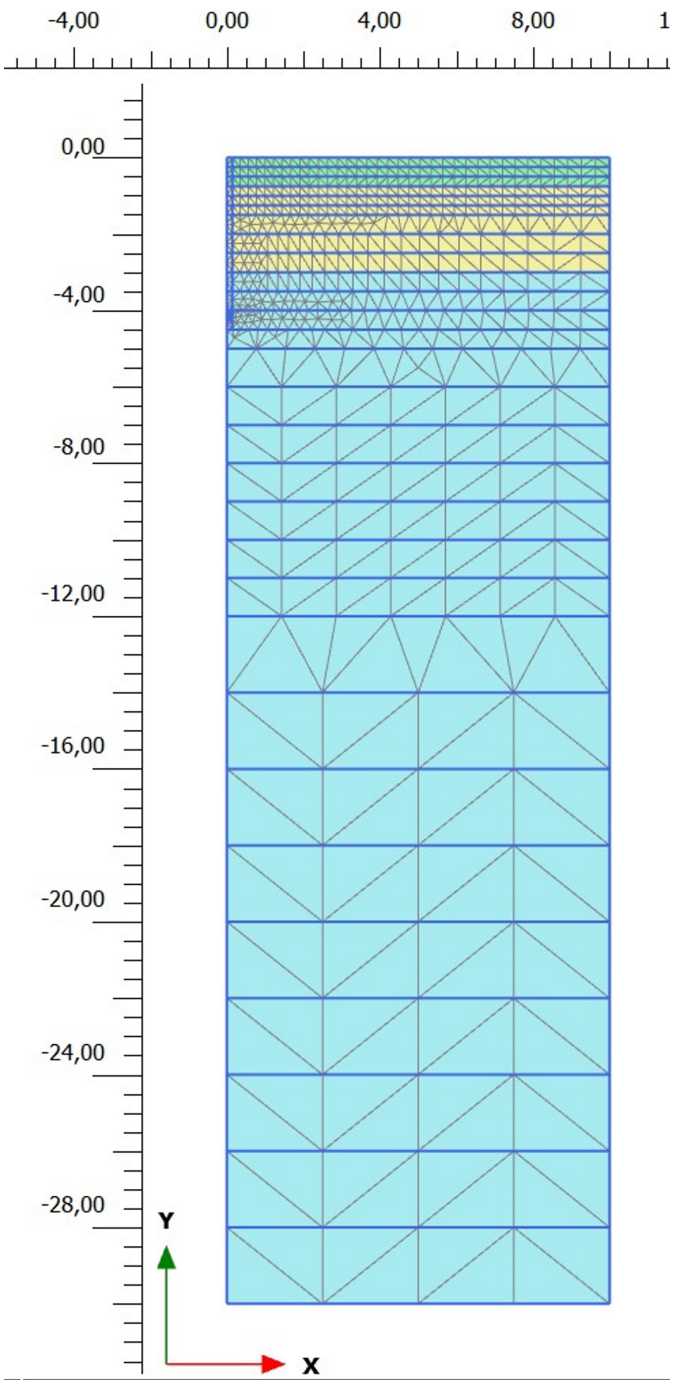

Figure 2: Modelled soil polygon and element mesh in PLAXIS.

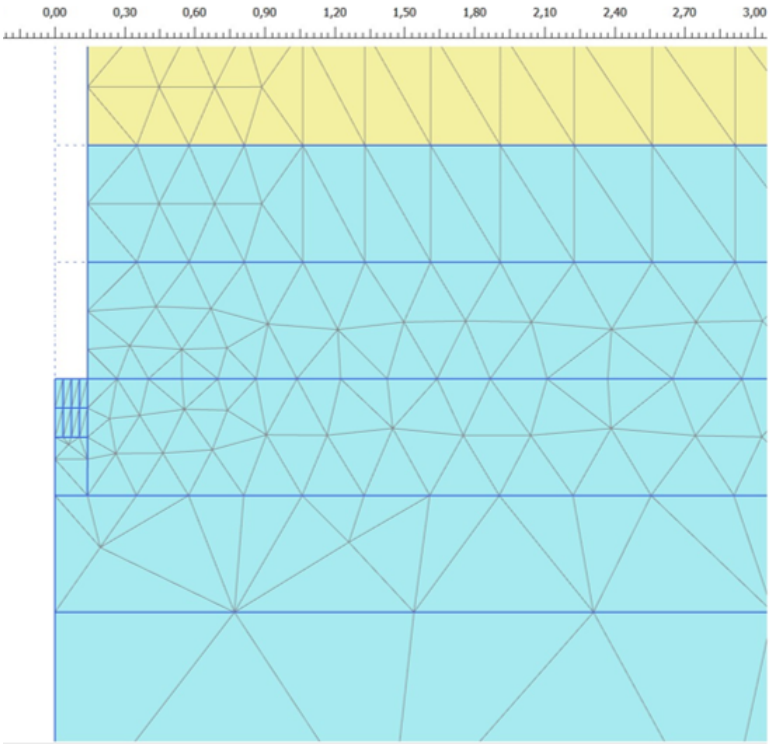

Figure 3: Modelled soil polygon and element mesh around the pile tip.

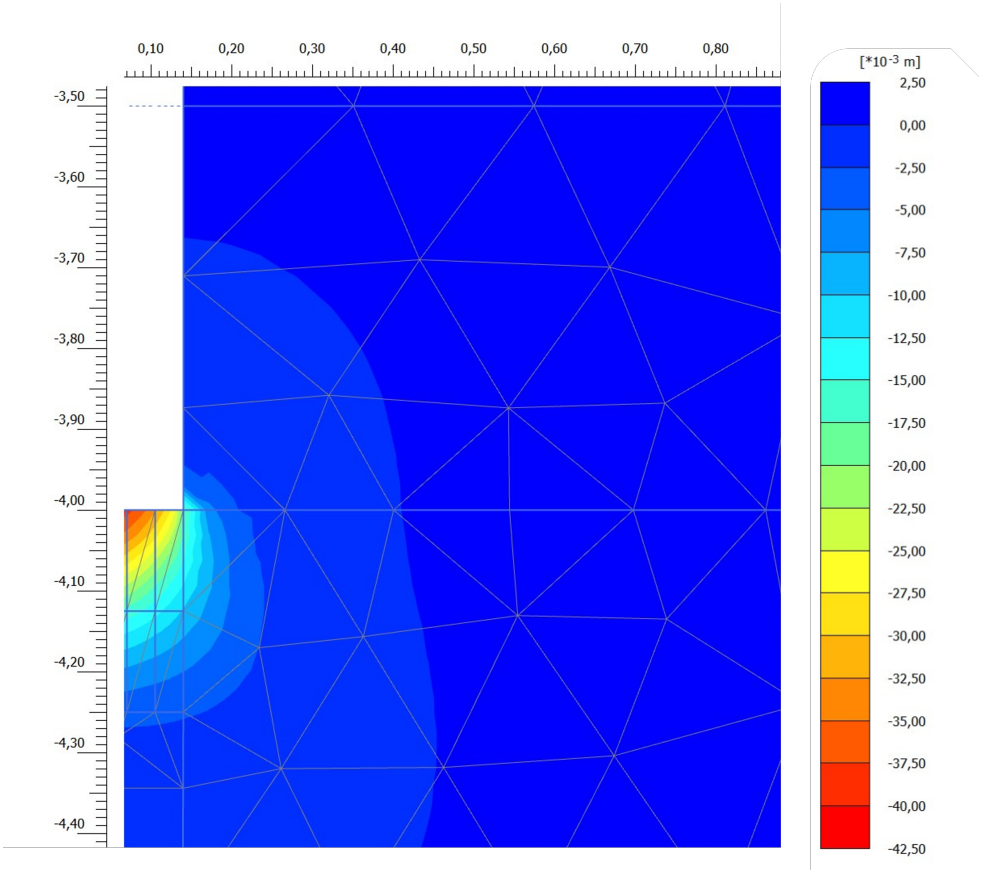

Figure 4: Vertical displacement around the pile tip for the soil polygon.

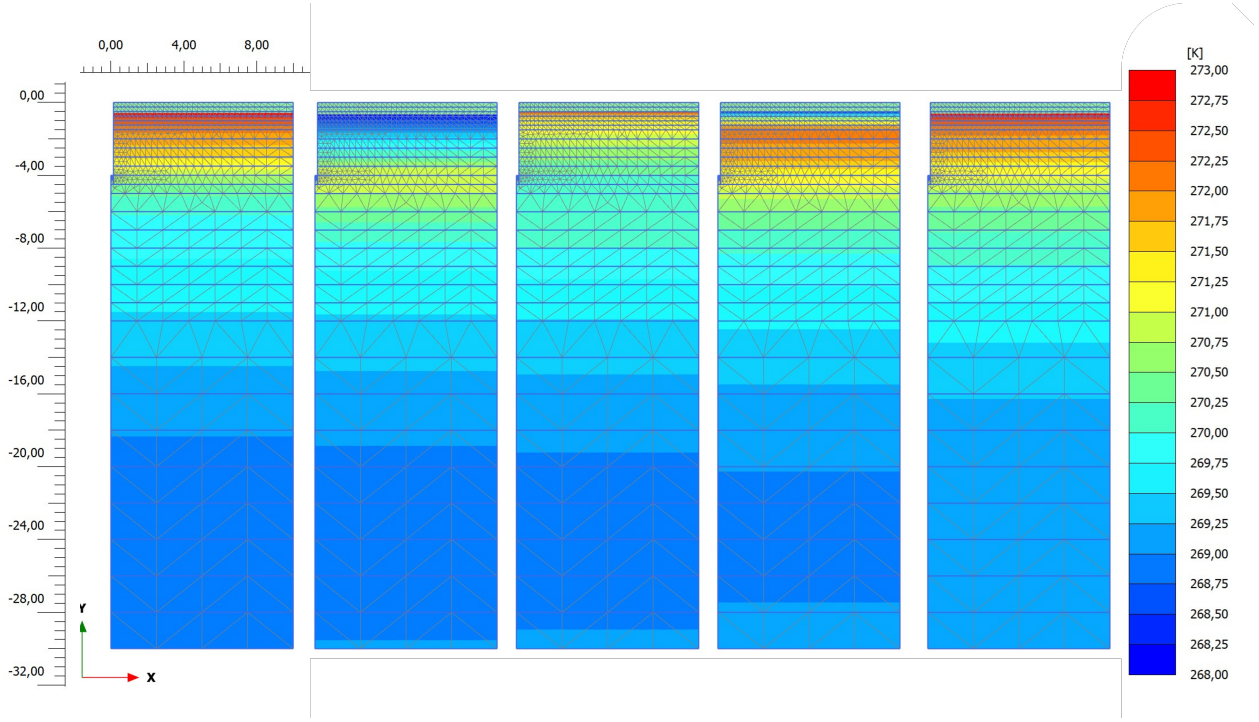

Figure 5: Temperature distribution through the soil polygon at the end of each creep phase, in ascending order from left to right.